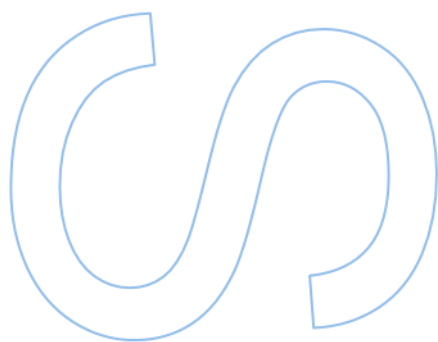
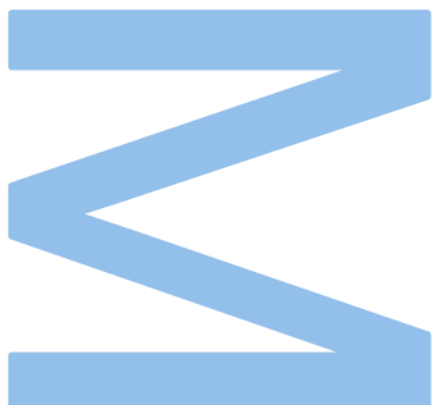


Study of the Development of a Lens Calibration Algorithm

U.PORTO
FEUP FACULDADE DE ENGENHARIA
UNIVERSIDADE DO PORTO

U.PORTO
FC FACULDADE DE CIÊNCIAS
UNIVERSIDADE DO PORTO

João Pedro da Silva Brito
Physics Engineering
Department of Physics and Astronomy
Faculty of Sciences of the University of Porto
2024/2025



Study of the Development of a Lens Calibration Algorithm

João Pedro da Silva Brito

Internship report carried out as part of the M.Sc. in Physics
Engineering
Department of Physics and Astronomy
2024/2025



Supervisor

Prof. José Costa Pereira, Assistant professor, Faculty of
Engineering of the University of Porto

External Supervisor in the Reception Entity

Guilherme Franco, AI Developer, wTVision

Acknowledgements

Abstract

WTVision, a business that specializes in real-time graphics and augmented reality solutions for the broadcast and entertainment industries, provided a corporate setting for this internship. With the use of WTVision's technology, immersive experiences that demand a high degree of visual accuracy and precision are produced. Accurate recreation of a camera lens distortion in a virtual environment is a major problem in these settings and an accurate determination of distortion coefficients is mandatory for recreating immersive AR experiences.

It's important to clarify that in augmented and virtual reality applications, where seamless alignment between virtual features and real-world visuals is necessary to deliver an immersive user experience, the aim is not to minimize the camera's distortion effect. Instead, the goal is to make the virtual world look geometrically aligned with the real world. However, current calibration methods are extremely time-consuming and require meticulous manual adjustments at different zoom and focus levels. Manual calibration typically takes between 4 to 8 hours and is heavily reliant on human factors, increasing the likelihood of errors.

The objective of this project is to create a lens calibration algorithm that optimizes and automates the procedure, cutting the overall calibration time down to about 30 minutes while maintaining accuracy. The suggested approach makes better use of cutting-edge methods like image analysis and machine learning to fix distortion issues. The study encompasses a thorough examination of current calibration techniques, the creation and modeling of a novel algorithm, and exhaustive experimentation on various types of lens under different circumstances.

The study's findings should greatly enhance the workflow for calibration teams by enabling faster, more accurate calibrations with less need for human intervention. The suggested method could significantly increase productivity in fields where accurate camera lens calibration is essential, especially for augmented and virtual reality applications.

Resumo

A WTVision é uma empresa especializada em soluções de gráficos em tempo real e realidade aumentada para a indústria de transmissão e entretenimento. A tecnologia da WTVision permite criar experiências imersivas que exigem um alto grau de precisão e exatidão visual. Um dos principais desafios nesses cenários é a recriação precisa da distorção de lentes de câmera em um ambiente virtual, sendo essencial a determinação acurada dos coeficientes de distorção para a criação de experiências imersivas de realidade aumentada.

É importante esclarecer que, em aplicações de realidade aumentada e virtual, onde o alinhamento perfeito entre elementos virtuais e imagens do mundo real é essencial para proporcionar uma experiência imersiva, o objetivo não é minimizar a distorção da câmera. Em vez disso, busca-se garantir que o mundo virtual esteja geometricamente alinhado com o mundo real. No entanto, os métodos atuais de calibração são extremamente demorados e exigem ajustes manuais meticulosos em diferentes níveis de zoom e foco. A calibração manual geralmente leva entre 4 a 8 horas e depende fortemente de fatores humanos, aumentando a probabilidade de erros.

O objetivo deste projeto é desenvolver um algoritmo de calibração de lentes que otimize e automatize o procedimento, reduzindo o tempo total de calibração para cerca de 30 minutos, sem comprometer a precisão. A abordagem proposta faz uso de técnicas avançadas, como análise de imagens e aprendizado de máquina, para corrigir problemas de distorção. O estudo abrange uma análise detalhada dos métodos atuais de calibração, o desenvolvimento e modelagem de um novo algoritmo e experimentações extensivas com diferentes tipos de lentes sob diversas condições.

Os resultados deste estudo devem melhorar significativamente o fluxo de trabalho das equipes de calibração, permitindo calibrações mais rápidas e precisas, com menor necessidade de intervenção humana. O método proposto pode aumentar substancialmente a produtividade em áreas onde a calibração precisa de lentes de câmera é essencial, especialmente em aplicações de realidade aumentada e virtual.

Contents

Acknowledgements	i
Abstract	ii
Resumo	iii
Contents	vii
List of Tables	viii
List of Figures	xi
Acronyms	xii
1 Introduction	1
1.1 Context	1
1.2 wTVision	2
1.3 Problem Definition and Internship Goals	3
1.3.1 Current Solution	3
1.3.2 Goals and Metrics	7
1.4 Document Overview	8

2 State of the Art	10
2.1 Understanding the Basics	10
2.1.1 What is augmented reality	10
2.1.2 What is Lens Distortion	11
2.1.3 What is the R^3 Software	13
2.2 Virtual Environment Calibration	13
2.2.1 Common Lens Distortion Problems	14
2.2.2 Types of Lens Distortion	14
2.2.3 Correcting Lens Distortion with OpenCV	15
2.2.4 Challenges in Using OpenCV for Virtual Environment Calibration	15
2.3 Communication Between Python and R^3	17
2.3.1 Why Sockets for Communication	17
2.3.2 Implementation Overview	17
2.3.3 Commands for Interaction with the Engine	18
2.3.3.1 Basic Engine Interaction Commands	18
2.3.3.2 Scene Export Commands	20
2.3.4 Benefits of Local Socket Communication	21
2.3.5 Applications and Future Potential	21
2.4 Deep Learning-Based Radial Distortion Estimation from a Single Image	22
2.4.1 The Brown–Conrady Radial Distortion Model	22
2.4.2 Learning-Based Single-Image Calibration	22
2.4.3 Proposed Implementation	23
2.5 Deep Learning-Based Image Deblurring	24

3 Edge Detection Using OpenCV	26
3.1 Canny Edge Detection	26
3.2 Using Blender for Testing	29
4 Camera Lens Calibration	35
4.1 Center-shift calibration	36
4.2 K1, K2 and Field of View (FoV) calibration	36
4.3 Calibration Scenarios	39
4.4 Results	40
5 Optimizing Calibration Efficiency	41
5.1 MockBoard	41
5.1.1 Communication with MockBoard	42
5.2 Results	43
6 Image Deblurring Using Neural Networks	46
6.1 Dataset	46
6.2 Deblurring using EDSR	47
6.3 Loss Function	47
6.3.1 MSELoss	47
6.3.2 The Structural Similarity Index (SSIM)	48
6.4 Mask Implementation	48
7 Deep Learning-Based Estimation of k_1 and k_2	50
7.1 Synthetic Dataset Generation	50
7.1.1 Source Images	51

7.1.2	Distortion Simulation	51
7.1.3	Supervision Labels	51
7.1.4	Training Process	52
7.1.5	Results	52
8	Conclusions and Future Work	54
9	Annexs	56
9.1	HTTP Headers	56
9.2	Calibration Results	57
	Bibliography	64

List of Tables

1.1 Calibration Times for Each Coefficient	6
9.1 HTTP Headers Used in the Request	56

List of Figures

1.1	Center shift calibration procedure example	5
1.2	FoV calibration procedure example	5
1.3	K1 calibration procedure example	6
1.4	Calibration Parameters	7
2.1	Example of an Augmented Reality (AR) scene developed by wTVision	11
2.2	Overlay used in the scene shown in Figure 2.1	11
2.3	Types of lens distortions: (a) Non-distortion, (b) Barrel distortion, (c) Pincushion distortion, (d) Mixed types of distortion	12
2.4	R^3 Space Designer interface	13
2.5	Example of a distorted image taken with a professional camera	14
2.6	Parallax Effect with the human eye. Left picture depicts a person's view with both eyes open. Right picture depicts the shift in perspective that occurs when one eye is closed.	16
3.1	Example of a canny edge detection application [1]	27
3.2	Image taken with the camera with the target at the center	28
3.3	Edge detection program demonstration	28
3.4	Loading a Scene	29
3.5	Adjusting Object Positions	30

3.6	Camera Positioning	31
3.7	Camera Lens Settings	32
3.8	Rendering the Image	32
3.9	Saving the Render	33
3.10	Edge Detection Results Visualization	34
4.1	Example of a center-shift calibration:(a) - Real object (red square) at max zoom, (b) - Insertion of a virtual cone with uncalibrated center-shift, (c) - Detection real object center coordinates, (d) - Calibrated virtual cone.	37
4.2	calibrated center-shift after changing the pan and tilt	37
4.3	Example of K1, K2 and Field of View (FoV) calibration using edge detection to determine the real object corners coordinates: (a) - FoV calibration, (b) - K1 calibration, (c) - K2 calibration.	38
4.4	Example of K1, K2 and FoV calibration using edge detection to determine the virtual object corners coordinates: (a) - FoV calibration, (b) - K1 calibration, (c) - K2 calibration.	39
4.5	Distortion calibration results	40
5.1	Selecting MockBoard as the output in the R^3 software.	42
5.2	MockBoard web page.	43
5.3	Distortion calibration results using the MockBoard.	44
5.4	Zoom 1 Focus 1 - (a) FoV, (b) K1, (c) K2.	45
6.1	Comparison between the original image and the masked result used for calibration.	49
7.1	Training loss (MSE) per epoch.	52
7.2	Distorted input (left) and rectified output (right) using predicted k_1 and k_2 . The CNN effectively compensates for radial distortion.	53

9.1	Zoom 1 Focus 1 - (a) FoV, (b) K1, (c) K2.	57
9.2	Zoom 1 Focus 2 - (a) FoV, (b) K1, (c) K2.	58
9.3	Zoom 2 Focus 1 - (a) FoV, (b) K1, (c) K2.	58
9.4	Zoom 2 Focus 2 - (a) FoV, (b) K1, (c) K2.	59
9.5	Zoom 3 Focus 1 - (a) FoV, (b) K1, (c) K2.	59
9.6	Zoom 3 Focus 2 - (a) FoV, (b) K1, (c) K2.	60
9.7	Zoom 4 Focus 1 - (a) FoV, (b) K1, (c) K2.	60
9.8	Zoom 4 Focus 2 - (a) FoV, (b) K1, (c) K2.	61
9.9	Zoom 5 Focus 1 - (a) FoV, (b) K1, (c) K2.	61
9.10	Zoom 5 Focus 2 - (a) FoV, (b) K1, (c) K2.	62
9.11	Zoom 6 Focus 1 - (a) FoV, (b) K1, (c) K2.	62
9.12	Zoom 6 Focus 2 - (a) FoV, (b) K1, (c) K2.	63
9.13	Zoom 7 Focus 1 - (a) FoV, (b) K1, (c) K2.	63

Acronyms

AR	Augmented Reality	CGI	Computer-generated imagery
VR	Virtual Reality		
FoV	Field of View	SSIM	The Structural Similarity Index

Chapter 1

Introduction

1.1 Context

Precise and dependable systems have become essential in an era where enterprises are driven toward more accuracy and efficiency by technology breakthroughs. The broadcast and entertainment industries have experienced significant expansion among these sectors due to the growing demand for immersive visual experiences enabled by Augmented Reality ([AR](#)) and Virtual Reality ([VR](#)) technologies. These innovations are transforming the way people consume material by providing them with interactive and captivating experiences. WTVision, a top business that specializes in real-time graphics and augmented reality solutions for many industries, is at the vanguard of this transformation.

The dynamic, aesthetically captivating settings that WTVision's technology helps creating for live broadcasts, sporting events, and virtual productions are essential. Achieving the desired level of realism that viewers anticipate requires a smooth transition between Computer-generated imagery ([CGI](#)) and real-world sights. But there are several obstacles in the way of reaching this level of visual accuracy, especially when it comes to camera lens calibration, which is essential to collecting real-world situations and matching them with virtual features.

In [AR](#) and [VR](#) settings, distortion can cause errors that impair the user experience. This difficulty is increased in apps that use varying zoom and focus settings since each one needs to be precisely calibrated in order to guarantee proper alignment of the virtual and real elements. At the moment, the labor and time-intensive process of calibrating camera lenses takes four to eight hours and involves manual adjustments. The repetitive nature of the work and human

mistake both make the process even more inefficient.

The limits of manual calibration approaches become more evident as the demand for AR and VR applications grows, especially in live broadcasts and virtual events. An automated solution that can speed up the calibration process and increase accuracy while decreasing time is desperately needed as a result of this. In light of this, the project's goal is to create a lens calibration algorithm that makes use of cutting-edge tools like image analysis and machine learning. The aim is to achieve maximum precision while radically reducing the time needed for the calibration process through automation and optimization.

The suggested method has the ability to greatly increase workflow efficiency in sectors that depend on accurately determined camera lens distortion coefficients by resolving these issues. wTVision is ideally positioned to spearhead this endeavor and shape the future of immersive broadcast experiences because to its experience with real-time graphics and augmented reality technologies. If this effort is successful, it could improve the visual quality of AR and VR material and establish new guidelines for lens calibration procedures in a variety of businesses.

1.2 wTVision

wTVision is a company specialized in creating integrated broadcasting solutions, focusing on software development, graphics design and live operations. Founded in 2001 and part of the Mediapro Group, wTVision has become a significant player in the broadcasting industry. The company provides a wide range of services, including real-time graphics, playout automation, augmented reality, virtual productions, and data distribution, serving live broadcasts, sports events, election coverage, entertainment shows, and news programs.

The company became one of the main real-time on-air graphics and playout automation providers due to its flexible solutions that can be integrated with multiple major graphics engines on the market. From small one time broadcasts to some of the most important competitions, wTVision takes part in more than 7 000 broadcasts annually and has experience in more than 120 countries. wTVision has hundreds of specialists around the globe and offices in Portugal, Spain, Belgium, Brazil, Bolivia, United Arab Emirates, India and USA.

Given that the sports industry is a primary focus for the company, and football is the dominant market in Portugal and many other countries, artificial intelligence and computer vision present

a wide range of new opportunities to be explored. As a result, this topic has been increasingly investigated by researchers over the past years.

1.3 Problem Definition and Internship Goals

This section presents a clear description of the current problem. This section will use the following fundamental concepts: **Augmented Reality AR**, **lens distortion** and the **R^3 software**. A detailed explanation of each can be found in chapter 2.

wTVision developed the R^3 software for creating virtual environments and integrating virtual objects into real scenes. This software enables augmented reality experiences by seamlessly introducing virtual elements into live footage. However, it does not account for lens distortion, meaning virtual objects remain undistorted while the real scene may exhibit natural optical warping. The challenge of this project is not to correct lens distortion but to accurately replicate it within virtual environments, ensuring a more realistic and cohesive augmented reality experience.

The limitations of the R^3 software, including its reliance on operator expertise, time-intensive calibration process, and lack of automation for dynamic zoom and focus adjustments, underscore the need for a more efficient solution.

This thesis aims to improve the calibration process by:

- Reducing reliance on operator expertise.
- Automating the process to decrease calibration time.

1.3.1 Current Solution

This section focuses on wTVision's current solution for calibrating a virtual environment, which involves using the R^3 software to distort the virtual environment to match the distortion observed in the real world.

While this approach is effective, the quality of the calibration—and, consequently, the realism of the virtual overlays—relies heavily on the calibration operator's experience and expertise. Additionally, it is a time-consuming process, typically taking between 4 to 6 hours.

Detailed Calibration Process

The calibration process involves determining the calibration coefficients in the following order:

- Center-shift
- Field of View
- k_1 (radial distortion)
- k_2 (radial distortion at the edges)
- Nodal Point

Calibration Preparation

Before starting the calibration process, the dimensions and coordinates of a real object on a real scene must be defined and provided to the R^3 software. This step can be completed either before or after the center-shift calibration. The following steps outline the calibration process for each coefficient:

1. **Center-Shift:** Align the virtual object with the real object at the center of the image. Adjust the central-shift coefficient until they match at minimum and maximum zoom levels. Figure 1.1 illustrates the current process for calibrating this coefficient. First, a real-world image with a reference point is required; typically, a phone light is used to produce the white circle in the image shown at the top of Figure 1.1. Next, a cone is introduced. This cone does not need any specific characteristics other than having a pointy end. The center-shift is then adjusted, as depicted, until the pointy end of the cone aligns with the center of the white circle of light. After achieving this alignment, zoom in and verify that the pointy end remains at the center of the circle of light. If not, readjust the center-shift accordingly.
2. **Field of View:** Move the real object (red square) off-center, then align the virtual object with the real object. Repeat this process for seven zoom levels to capture variations in distortion. Figure 1.2 illustrates the calibration procedure for a FoV.
3. **k_1 and k_2 :** Move the object to the edges of the frame. Adjust k_1 and k_2 coefficients until alignment is achieved. Repeat across all zoom levels. Figure 1.3 illustrates the K1



Figure 1.1: Center shift calibration procedure example



Figure 1.2: FoV calibration procedure example

calibration. The K2 calibration is analog to the K1 calibration, however the real object should be moved to the corner of the image. Figure 1.4 illustrates where the object needs to be for each specific coefficient calibration.

4. **Nodal Point:** Follow the steps to align two reference objects at different depths, ensuring



Figure 1.3: K1 calibration procedure example

there is **no parallax effect**¹ when the camera rotates slightly.

Challenges of Current Method

The current solution is effective, but it has limitations:

- Time-intensive calibration process.

Coefficient	Calibration Time (min)
Center-shift	5 - 10
FoV	60 - 120
K1	60 - 120
K2	60 - 120
Nodal	60 - 120

Table 1.1: Calibration Times for Each Coefficient

- Reliance on operator expertise for accurate results.
- Lack of automation for dynamic zoom and focus adjustments.

¹The **no parallax effect** occurs when a camera rotates around its *nodal point*, preventing any apparent shift between foreground and background objects. This ensures that elements at different depths remain perfectly aligned, eliminating unwanted distortions caused by parallax. Achieving this effect is crucial for seamless panoramic photography and precise image stitching, as it allows multiple frames to blend naturally without misalignment.

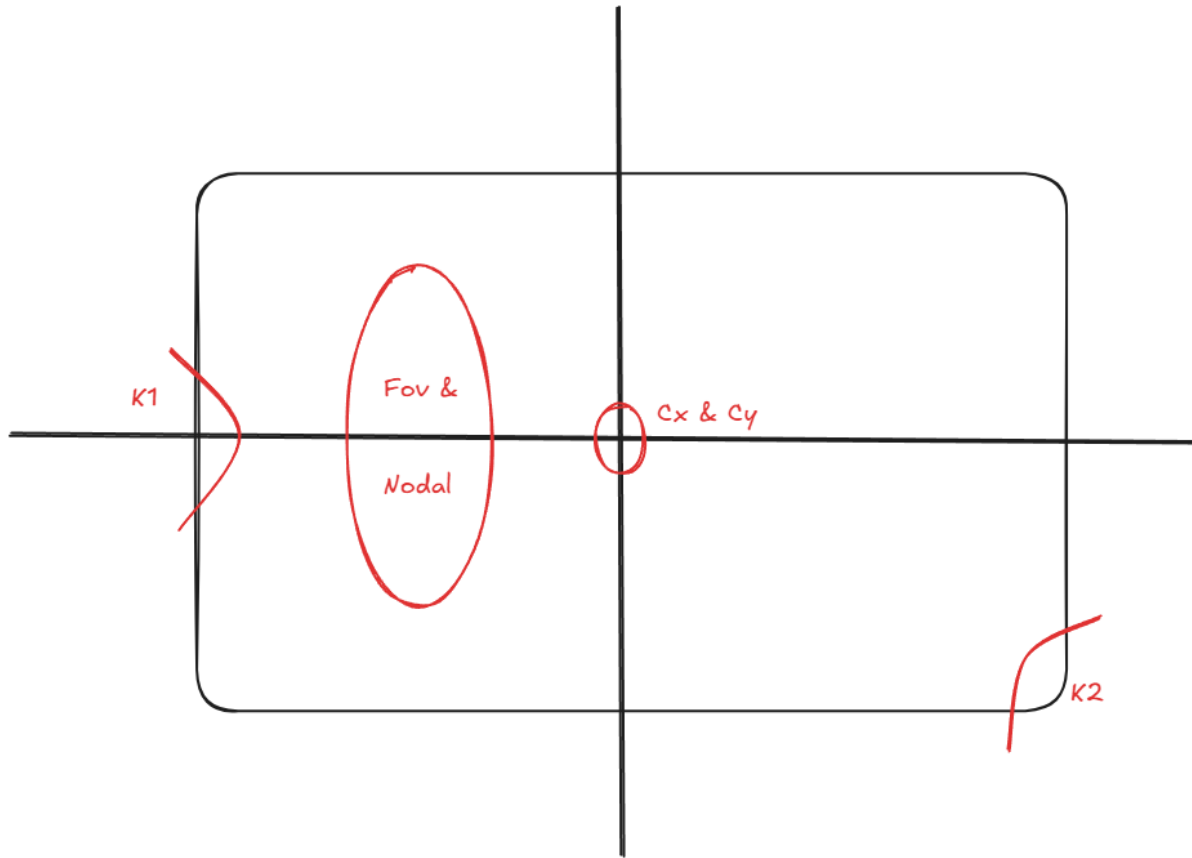


Figure 1.4: Calibration Parameters

1.3.2 Goals and Metrics

The primary goal of this project is to improve the calibration process, making it faster, more reliable, and less dependent on the expertise of the operator. The success of this solution will be evaluated based on:

1. **Accuracy of distortion coefficient estimation relative to manual calibration.** The performance of the model will be assessed by simulating images with known distortion parameters using the R^3 software and comparing the experimental values to these ground truth coefficients. The target is to achieve a relative error of less than 5% for k_1 , the field of view (FoV) and center-shift. For the k_2 coefficient, a higher tolerance of up to 10% is acceptable².
2. **Reduction in calibration time.** The goal is to reduce the calibration time to 30 minutes

²The k_2 coefficient is considered less critical for most calibration tasks. According to field operators, k_2 is sometimes neglected during manual calibration when time is constrained, as its inclusion offers limited qualitative improvement.

or less.

3. **Consistency across multiple zoom and focus levels.** Which will be measured by analyzing multiple zoom and focus levels and comparing the results.
4. **Automation of the calibration process.** The goal is to automate the calibration process as much as possible, reducing the need for manual adjustments.

1.4 Document Overview

This thesis is organized into several chapters, each addressing a different component of the proposed solution for camera calibration and the associated image processing tasks. The structure of the document is as follows:

- **Chapter 1 – Introduction:** Introduces the context and motivation behind this work, highlighting the challenges of manual camera calibration in augmented reality systems and defining the objectives and scope of the project.
- **Chapter 2 – State of the Art:** Introduces foundational concepts in augmented reality and camera lens distortion, followed by a review of tools like OpenCV and wTVision’s R³ software. Explores the limitations of traditional calibration methods, details socket-based communication with R³, and surveys recent advances in deep learning-based image deblurring, establishing the technological background for this work.
- **Chapter 3 – Edge Detection Using OpenCV:** Describes the implementation of edge detection techniques using OpenCV to identify target corners and centroids for AR camera calibration. Highlights the application of the Canny edge detection algorithm and Blender-based synthetic image generation for testing. Explores the methodology, benefits, and challenges, including limitations encountered in real-world scenarios and adjustments made to improve detection accuracy.
- **Chapter 4 – Camera Lens Calibration:** Presents an iterative algorithm for determining distortion coefficients in AR camera systems, using virtual test images with known parameters. Details the calibration procedures for center-shift, FoV, and distortion coefficients K_1 and K_2 , emphasizing accuracy and alignment methods. Highlights practical challenges, such as processing time, and outlines three calibration scenarios encountered during testing.

- **Chapter 5 – Optimizing Calibration Efficiency:** Investigates methods to reduce the runtime of the calibration algorithm, focusing on system-level bottlenecks. Details the transition from file-based image handling to real-time image transfer using wTVision’s MockBoard, a virtual graphics card. Demonstrates how this change significantly improves performance, cutting calibration time by over 70% while maintaining accuracy.
- **Chapter 6 – Image Deblurring Using Neural Networks:** Explores the use of neural networks to restore image sharpness for improved camera calibration accuracy. Describes the training process using synthetic blurred data and the application of the EDSR model. Evaluates different loss functions and proposes a masking strategy as a practical workaround for mild blur, laying the groundwork for future enhancements.
- **Chapter 7 – Deep Learning-Based Estimation of k_1 and k_2 :** Describes a neural network approach for estimating distortion coefficients from a single image without calibration targets. Trained on synthetic data using the Brown–Conrady model, the system achieves under 5% error for k_1 and under 10% for k_2 , offering a fast and flexible alternative to traditional methods.
- **Chapter 8 – Conclusions and Future Work:** Summarizes the development of an automated AR camera calibration algorithm that reduces operator dependency and runtime while maintaining high accuracy. Highlights key contributions such as distortion estimation, MockBoard-based optimization, and preliminary work in neural network deblurring. Outlines future directions including real-time calibration, enhanced deep learning methods, and full system automation.

Chapter 2

State of the Art

2.1 Understanding the Basics

Before diving into a detailed explanation, it is essential to understand some foundational concepts. The following sections provide simplified explanations of these key concepts:

1. What is Augmented Reality ([AR](#)) ?
2. What is lens distortion?
3. What is the R^3 software?

2.1.1 What is augmented reality

[AR](#) is a technology that overlays digital information—such as images, sounds, or text—onto the real world. Unlike Virtual Reality ([VR](#)), which creates a fully immersive digital environment, [AR](#) enhances reality by adding interactive, computer-generated elements. For example, in mobile applications or games like Pokémon GO, digital characters appear as if they are part of the physical world when viewed through the device's camera. [AR](#) is used in various fields, including gaming, retail, education, and training, to enrich the user experience with additional layers of digital content.

wTVision implements [AR](#) on video streaming platforms. Figures [2.1](#) and [2.2](#) show a frame from a video of an [AR](#) scene developed by wTVision.



Figure 2.1: Example of an AR scene developed by wTVision



Figure 2.2: Overlay used in the scene shown in Figure 2.1

2.1.2 What is Lens Distortion

In ideal pinhole cameras, straight lines in the world project as straight lines in the image. However, real optical lenses introduce geometric aberrations that violate this principle. Among these, *radial distortion* arises due to the nonlinear refraction of light rays at increasing angles of incidence—an

effect governed by principles of geometric optics. This manifests in images as the curvature of lines that should be straight, particularly near the image periphery.

Barrel distortion ($k_1 < 0$) causes lines to bulge outward, while pincushion distortion ($k_1 > 0$) compresses lines inward. These effects are particularly prominent in wide-angle lenses due to their higher field-of-view, where off-axis rays undergo stronger deviation due to lens curvature and gradient-index profiles. Figure 2.3 illustrates various types of lens distortion.

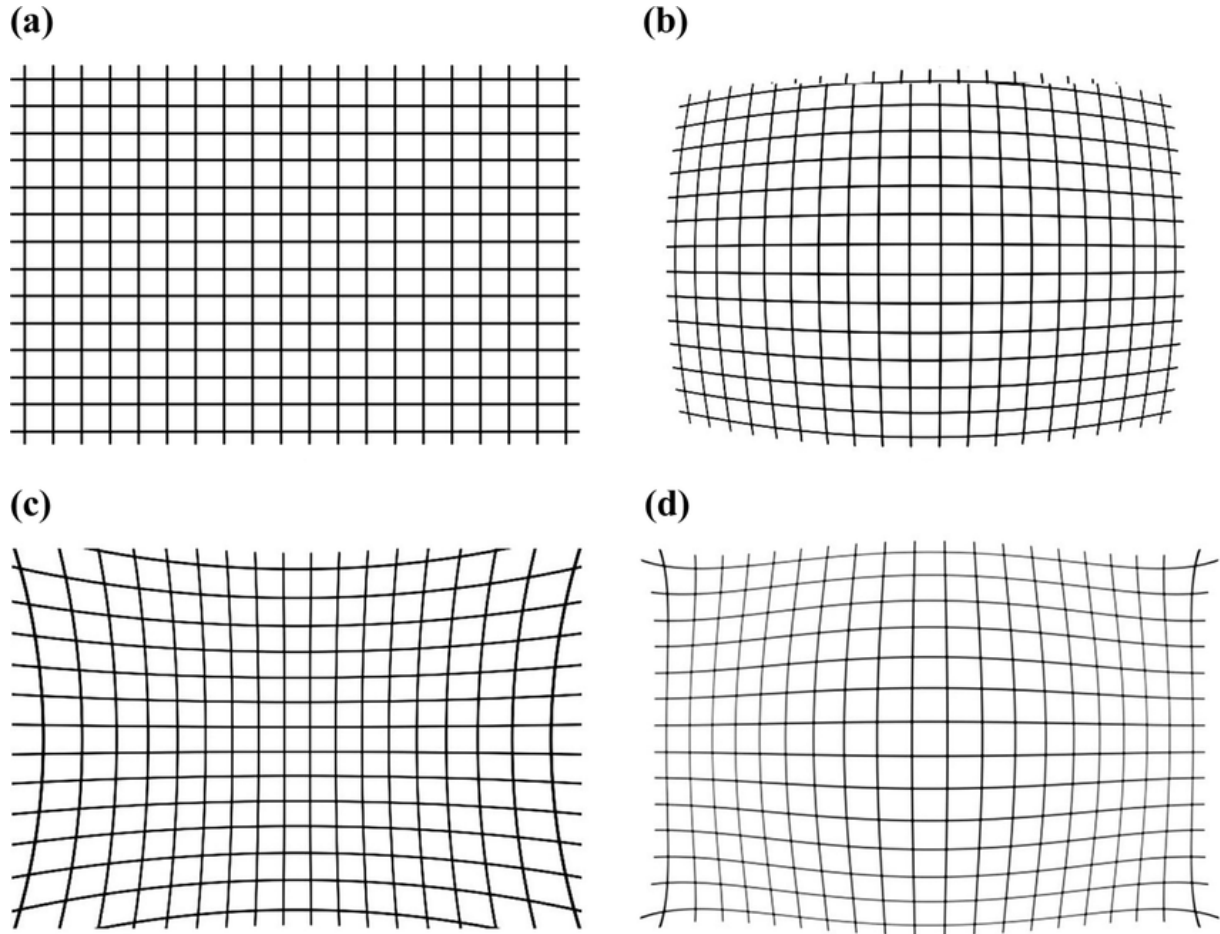


Figure 2.3: Types of lens distortions: (a) Non-distortion, (b) Barrel distortion, (c) Pincushion distortion, (d) Mixed types of distortion

Cameras used by wTVision have some degree of distortion, although it is not very noticeable. However, when inserting virtual overlays in a video, it is crucial to distort the virtual environment in the same way the camera lens distorts the real world. This ensures that virtual objects appear realistic and correctly aligned. Without this distortion, virtual objects would appear out of place when inserted into the real-world scene.

2.1.3 What is the R^3 Software

To address this issue, wTVision developed the R^3 software. This tool includes an engine and a software platform that provides the necessary technology to create and render digital environments. Within the platform, the "Space Designer" tool allows developers to build, layout, and arrange the virtual environment where the interactive experience takes place. While the engine handles rendering graphics, processing physics, and managing assets, the Space Designer offers an interactive, visual interface for creating the look and feel of the virtual world. Figure 2.4 shows the R^3 Space Designer interface.

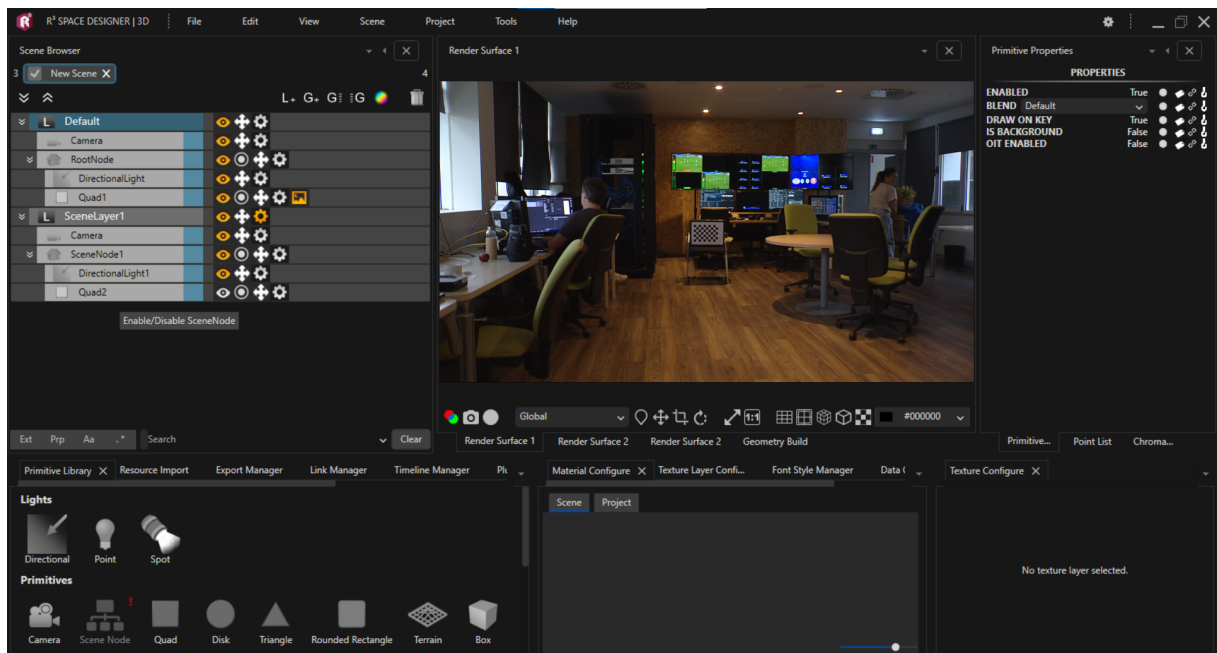


Figure 2.4: R^3 Space Designer interface

2.2 Virtual Environment Calibration

Earlier, we mentioned that wTVision developed the R^3 software to calibrate the virtual environment. This section explains why they developed a specialized tool instead of using existing tools like OpenCV for determining rectification coefficients, and it examines the pros and cons of the software.

2.2.1 Common Lens Distortion Problems

First, let's clarify how typical lens distortion issues are handled. For example, photographers using professional cameras frequently encounter distorted images, as shown in Figure 2.5.



Figure 2.5: Example of a distorted image taken with a professional camera

To correct these distortions, the OpenCV library is often used by applying specific distortion coefficients.

The main types of lens distortion are **Radial Distortion** and **Tangential Distortion**. Each type has distinct causes and visual effects, which are explained below.

2.2.2 Types of Lens Distortion

- **Radial Distortion:**

Radial distortion occurs when light rays bend unevenly as they pass through the lens, causing straight lines to appear curved. This distortion is more pronounced at the image edges and is mathematically described by:

$$x_{\text{distorted}} = x \left(1 + k_1 r^2 + k_2 r^4 + k_3 r^6 \right) \quad (2.1)$$

$$y_{\text{distorted}} = y \left(1 + k_1 r^2 + k_2 r^4 + k_3 r^6 \right) \quad (2.2)$$

where k_1 , k_2 , and k_3 are radial distortion coefficients, and r represents the distance from the optical center.

- **Tangential Distortion:**

Tangential distortion results from misalignment between the camera sensor and the lens, causing image points to shift in a direction based on their position. This distortion is modeled by:

$$x_{\text{distorted}} = x + \left[2p_1 xy + p_2 \left(r^2 + 2x^2 \right) \right] \quad (2.3)$$

$$y_{\text{distorted}} = y + \left[p_1 \left(r^2 + 2y^2 \right) + 2p_2 xy \right] \quad (2.4)$$

where p_1 and p_2 are tangential distortion coefficients.

2.2.3 Correcting Lens Distortion with OpenCV

To correct these distortions, OpenCV uses a set of distortion coefficients. The five main coefficients— k_1 , k_2 , p_1 , p_2 , and k_3 —capture both radial and tangential distortion effects:

$$\text{Distortion Coefficients} = \begin{pmatrix} k_1 & k_2 & p_1 & p_2 & k_3 \end{pmatrix} \quad (2.5)$$

OpenCV can use these coefficients to rectify distorted images.

2.2.4 Challenges in Using OpenCV for Virtual Environment Calibration

As mentioned, this project does not aim to rectify images but to calibrate the geometry of a virtual environment. For this, we need to determine the camera's distortion coefficients.

OpenCV calculates distortion coefficients like k_1 , k_2 , p_1 , p_2 , and k_3 to correct image distortion.

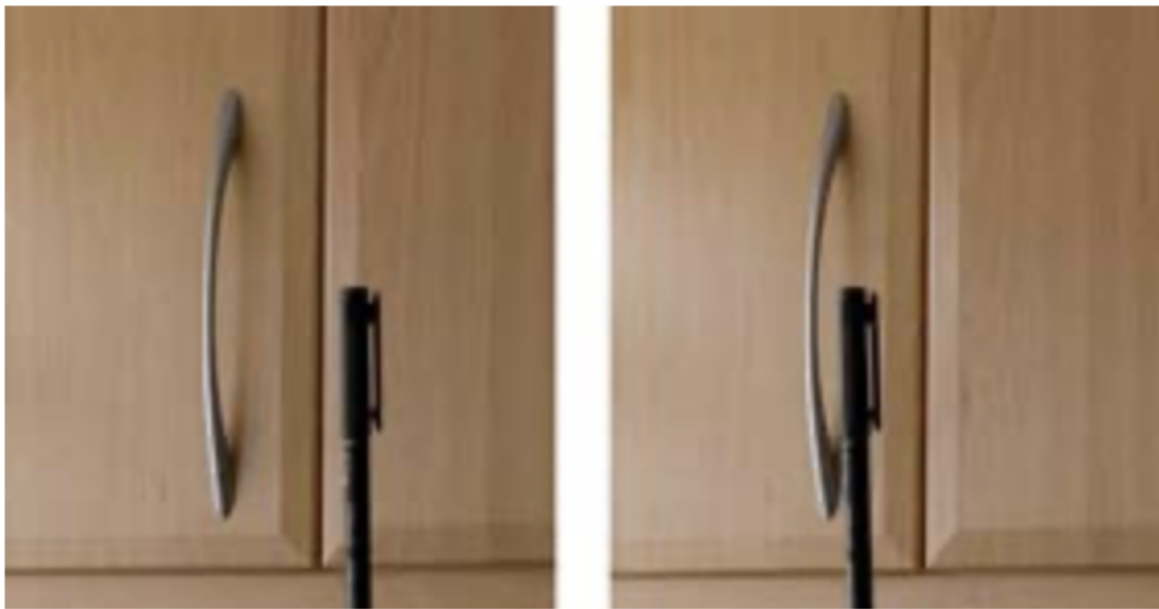


Figure 2.6: Parallax Effect with the human eye. Left picture depicts a person's view with both eyes open. Right picture depicts the shift in perspective that occurs when one eye is closed.

However, for our specific needs, additional coefficients are required that OpenCV cannot provide:

- **Central-Shift:** Due to misaligned lenses, the real-world origin point $(0,0,0)$ and the virtual one may differ, necessitating a central-shift coefficient.
- **No Parallax Effect Coefficient:** To achieve the No Parallax Effect, the virtual environment must behave similarly to the camera, with minimized parallax. The No Parallax Effect coefficient aims to eliminate the apparent shift in object positions due to a viewpoint change. Figure 2.6 illustrates this phenomenon. The first image depicts a person's view with both eyes open, offering a complete perspective of the object. In contrast, the second image illustrates the shift in perspective that occurs when one eye is closed, significantly altering the perception of the object.
- **Field of View (FoV):** The **field of view (FOV)** is the extent of the scene captured by the camera, measured in degrees. It depends on the focal length and sensor size, with wider angles covering more of the scene and narrower angles focusing on a smaller area. Adjusting the camera's zoom changes the FoV, alters the perceived distance of objects. Replicating this effect in AR requires altering the FoV in the virtual environment.

2.3 Communication Between Python and R^3

In this work, the communication between Python and the R^3 software is implemented using sockets. Sockets are a fundamental mechanism in computer systems that enable processes to exchange data. While traditionally used for communication over a network, sockets can also be employed to facilitate communication between processes on the same machine, leveraging the system's networking stack for local inter-process communication (IPC) [2, 3].

2.3.1 Why Sockets for Communication

Sockets provide a simple and robust interface for connecting applications written in different programming languages. In this case, Python acts as the controlling script, orchestrating the execution of the R^3 software. Using sockets offers the following advantages:

- **Language Agnosticism:** Python and R^3 operate independently, and sockets enable communication without requiring language-specific bindings or modifications to the software [4, 5].
- **Asynchronous Communication:** Sockets allow Python to send commands to R^3 and wait to receive responses at different rates, enabling efficient two-way communication [2].
- **Local Communication:** Although sockets are often associated with network communication, they can be used for local IPC by binding the socket to the loopback interface (localhost). This ensures that all communication remains within the same machine, minimizing latency and security concerns [3].

2.3.2 Implementation Overview

The implementation of the communication relies on a server-client model [4]:

1. **Socket Initialization:** A socket initialized in Python connects it to the R^3 software, configured as the server, and bound to a specific port (9009) on the loopback address (127.0.0.1) [5].
2. **Connection from R^3 :** Python acts as a client, connecting to R^3 .

3. **Message Exchange:** Once connected, Python sends commands or data to R^3 , and the latter processes the instructions and responds via the same socket [2].
4. **Closing the Connection:** After the data exchange is complete, the connection is gracefully closed, releasing resources.

2.3.3 Commands for Interaction with the Engine

The communication between Python and the R^3 software, as outlined in Section 2.3, enables the execution of specific commands to interact with the engine's functionality. Below, we describe the key commands used in this implementation, their purposes, and their syntax, as demonstrated in the provided examples.

2.3.3.1 Basic Engine Interaction Commands

- **TakeSnapshot:** This command captures a snapshot of the render surface and saves it as a PNG image. The default save location is the "Projects" folder, but users can specify a custom path and filename. The command supports two syntaxes:
 - `engine.takeSnapshot "file_name"`: Saves the snapshot with the specified filename in the default "Projects" folder.
 - `engine.takeSnapshot "path_with_filename"`: Saves the snapshot at the specified path with the given filename.

Upon success, the engine responds with "OK: SNAPSHOT TAKEN". If an invalid path is provided, it returns an error message: "ERROR: SNAPSHOT – INVALID PATH". For example:

```
engine.takeSnapshot "JornalNoiteTicker"
```

saves a snapshot named "JornalNoiteTicker.png" in the default location, while:

```
engine.takeSnapshot "C:/Users/john.doe/Desktop/JornalNoiteTicker"
```

saves it to a specific desktop path.

- **GetSnapshot:** This command retrieves a snapshot previously taken with TakeSnapshot and returns it as a base64-encoded string. It is essential to use TakeSnapshot before invoking GetSnapshot, as the latter relies on the existence of a snapshot file. The command supports two syntaxes:

- engine.getSnapshot "file_name": Retrieves the snapshot with the specified filename from the default "Projects" folder.
- engine.getSnapshot "path_with_filename": Retrieves the snapshot from the specified path and filename.

Upon success, the engine responds with:

```
"OK: <IMAGE> base64string <IMAGE>"
```

If the snapshot file cannot be found or the path is invalid, it returns an error message, such as:

```
"ERROR: GETSNAPSHOT - COULD NOT READ LAST SNAPSHOT FILE"  
"ERROR: GETSNAPSHOT - INVALID PATH"
```

For instance:

```
engine.getSnapshot "JornalNoiteTicker"
```

returns the base64-encoded image data for the snapshot named "JornalNoiteTicker.png" in the default location.

- **Get:** This command retrieves the current tracking packet from a specified tracking camera, providing detailed camera parameters and status. The syntax is:

```
engine.tracking "tracking_camera_name" get
```

Upon success, the engine responds with:

```
"OK: CURRENT CAMERA PARAMETERS:"
```

followed by a JSON-like structure containing parameters such as field of view (FovX, FovY), aspect ratio, position (PosX, PosY, PosZ), rotation (RotX, RotY, RotZ), and other metadata like view matrix, center coordinates, and sensor size. For example:

```
engine.tracking "Cam0" get
```

might return a response detailing the parameters of the "Cam0" tracking camera, including:

```
"FovX": 80.0, "FovY": 50.0, ...
```

2.3.3.2 Scene Export Commands

In addition to the basic engine interaction commands, the system supports a set of more complex *Scene Export* commands for managing and manipulating scene properties within R^3 . These commands operate on export entities (e.g., properties like transform positions, scales, or text values) and can be executed individually or in batches (via *MultiExport*). Below, we detail each command and its functionality:

- **SetValue:** This command sets the value of a specific export property within a scene. The syntax is:

```
scene "project_ref/scene_ref" export "export_name" SetValue "value"
```

- **Rename:** This command renames an existing export within a scene. The syntax is:

```
scene "project_ref/scene_ref" export "export_name" rename "new_name"
```

- **GetValue:** This command retrieves the current value of a specific export property within a scene. The syntax is:

```
scene "project_ref/scene_ref" export "export_name" getValue
```

- **MultiExport Commands:** These commands allow batch operations on multiple exports.

Example:

```
scene "JornalNoite/teste" export "transform.scale" SetValue "1,2,1"
      "text" SetValue "player_name" "alpha" SetValue "0.5"
```

returns:

```
"OK: SCENE EXPORT SETVALUE - Value Set."
"OK: SCENE EXPORT SETVALUE - Value Set."
"OK: SCENE EXPORT SETVALUE - Value Set."
```

These *Scene Export* commands provide fine-grained control and automation through Python scripts, enabling efficient real-time scene manipulation.

2.3.4 Benefits of Local Socket Communication

By utilizing sockets for communication between Python and R^3 , this setup ensures modularity and scalability. Python and R^3 remain decoupled, allowing for independent updates or replacements of either component without affecting the communication protocol. Additionally, the use of the loopback interface ensures that no external networking hardware or configuration is required [3].

2.3.5 Applications and Future Potential

This socket-based architecture facilitates a variety of use cases, such as:

- Automating tasks in R^3 through Python scripts.
- Integrating Python's data analysis and visualization capabilities with R^3 's functionality.
- Enabling real-time monitoring and feedback loops between Python and R^3 .

In summary, the use of sockets for communication between Python and R^3 provides a flexible and efficient solution for inter-process communication, paving the first step to automate the lens calibration.

2.4 Deep Learning-Based Radial Distortion Estimation from a Single Image

Calibrating a camera from a single image without known geometry is a challenging task. Recent advances in deep learning enable convolutional neural networks (CNNs) to estimate intrinsic parameters directly from image content by learning patterns associated with lens distortion. These models exploit visual cues such as curvature and spatial deformation to regress distortion coefficients like k_1 and k_2 , even in unstructured scenes.

2.4.1 The Brown–Conrady Radial Distortion Model

A widely adopted model to describe lens distortion is the Brown–Conrady model [6], which decomposes distortion into radial and tangential components. For many practical applications, tangential components are negligible, and only the radial terms are retained. The distorted coordinates (x_d, y_d) are expressed as:

$$\begin{aligned} x_d &= x \left(1 + k_1 r^2 + k_2 r^4 \right), \\ y_d &= y \left(1 + k_1 r^2 + k_2 r^4 \right), \end{aligned} \tag{2.6}$$

where $r = \sqrt{x^2 + y^2}$ is the radial distance from the image center, and k_1, k_2 are the distortion coefficients. These terms model second- and fourth-order distortion, and are dimensionless when coordinates are normalized by focal length. In optical terms, they encode higher-order transverse aberrations and vary with lens geometry and refractive index distribution.

2.4.2 Learning-Based Single-Image Calibration

Recent work in computer vision has applied deep learning to the problem of intrinsic parameter estimation from a single image [7–9]. Convolutional neural networks (CNNs) are capable of regressing distortion coefficients by identifying subtle cues such as curved edges, radial stretching,

and characteristic perspective warping.

To enable training, large synthetic datasets are generated by applying known distortions to undistorted images using forward models based on Eq. (1). Each distorted image is paired with its known (k_1, k_2) , providing supervision for training.

This method avoids the need for calibration targets and enables on-the-fly estimation of distortion in the wild. Recent models such as Lopez-Antequera *et al.* [9] use synthetic data derived from panoramic images and regress both intrinsic and extrinsic parameters.

2.4.3 Proposed Implementation

In this work, we implement a CNN-based distortion estimator that directly regresses k_1 and k_2 from a single distorted RGB image. The network uses a ResNet-18 backbone [10], pretrained on ImageNet and fine-tuned on a custom synthetic dataset.

Training images are 256×256 pixels, synthetically distorted using the Brown–Conrady model with coefficients sampled from:

$$k_1 \sim \mathcal{U}(-0.4, 0.4), \quad k_2 \sim \mathcal{U}(-0.2, 0.2). \quad (2.7)$$

The training loss is the mean squared error (MSE) between predicted and true coefficients:

$$\mathcal{L} = \frac{1}{2} \left[(k_1^{\text{pred}} - k_1^{\text{true}})^2 + (k_2^{\text{pred}} - k_2^{\text{true}})^2 \right]. \quad (2.8)$$

This approach allows the model to learn a physical mapping from image features to distortion coefficients without relying on explicit geometry or calibration targets.

Although small deviations from ground truth remain, especially for extreme distortions or textureless regions, this method represents a powerful alternative for intrinsic calibration in scenarios where traditional methods fail.

2.5 Deep Learning-Based Image Deblurring

Deep learning has significantly advanced the field of image deblurring, providing powerful alternatives to traditional deconvolution methods. Convolutional Neural Networks (CNNs) form the basis of many state-of-the-art approaches. Early CNN-based models, such as those proposed by Sun et al. [11], showed promise in handling non-uniform motion blur using data-driven learning.

A major milestone came with the work of Nah et al. [12], who introduced a multi-scale CNN that operates in a coarse-to-fine manner. This architecture effectively addressed the challenge of spatially variant blur by progressively refining image details at increasing resolutions. Tao et al. [13] further improved this design by proposing the Scale-Recurrent Network (SRN), which reuses network weights across multiple scales, enhancing both efficiency and accuracy.

Residual learning has played a central role in the performance of modern deblurring models. The SRResNet architecture, introduced by Ledig et al. [14] for super-resolution, inspired several deblurring variants by incorporating deep residual blocks and removing batch normalization. EDSR (Enhanced Deep Super-Resolution), proposed by Lim et al. [15], further optimized this concept by expanding network depth and capacity, leading to state-of-the-art results in image restoration.

Another significant development is the use of adversarial learning frameworks. Kupyn et al. [16] introduced DeblurGAN, which models deblurring as a conditional image-to-image translation problem. It employs a GAN loss, along with a perceptual loss computed from VGG feature maps [17], to improve the realism of reconstructed images. This approach enhances high-frequency detail reconstruction and perceptual quality. DeblurGAN-v2 [18] refined this concept using a feature pyramid generator and more efficient training strategies, achieving faster and more accurate results.

Loss function design is critical in deblurring networks. While Mean Squared Error (MSE) is widely used for optimizing pixel fidelity, it often leads to overly smooth results [19]. Alternatives like Mean Absolute Error (MAE) or the Charbonnier loss can better preserve edges. Structural Similarity Index (SSIM) [20] loss, formulated as $L_{\text{SSIM}} = 1 - \text{SSIM}$, captures luminance, contrast, and structural information, offering perceptual advantages. Furthermore, perceptual loss functions [17], which compare deep feature representations instead of raw pixels, have proven effective for

preserving semantic content during deblurring.

Recently, attention mechanisms and transformer-based models have further pushed the boundaries of performance. Models like Uformer [21] and Restormer [22] utilize self-attention to model long-range dependencies, resulting in higher PSNR and SSIM scores on standard benchmarks such as GoPro.

Overall, the progression from CNNs to GANs, and now to Transformer-based architectures, reflects the evolution of deep learning approaches in addressing the complex task of image deblurring.

Chapter 3

Edge Detection Using OpenCV

The internship project began with the final objective of automating the Augmented Reality ([AR](#)) camera lens calibration. For that, the following tasks were outlined:

1. Develop a program that detects the coordinates (in pixels) of the corners of a quadrilateral target, as well as the corresponding centroid.
2. Using the centroid coordinates, calibrate the central-shift.
3. Using the coordinates of the corners of the target, calibrate the FoV and k_1/k_2 coefficients.
4. Calibrate the nodal point.

The objective is to recreate the calibration procedure that an operator uses. The following sections explain in detail how each task is completed, as well as the limitations and advantages of the current methods.

3.1 Canny Edge Detection

Even though OpenCV cannot directly provide the coefficients required, this library still proves useful for its powerful image object detection functions.

Canny edge detection is a multi-step algorithm designed to detect a wide range of edges in images. It begins with noise reduction—typically using a Gaussian filter—to smooth the image and minimize the impact of noise. Next, the algorithm computes the intensity gradients to identify areas with rapid intensity changes, which serve as potential edge locations. To refine

these candidate edges, non-maximum suppression is applied to thin the detected edges, ensuring that only the strongest responses are retained. Finally, double thresholding and edge tracking by hysteresis are used to classify edges as strong or weak, and to connect weak edges that are likely part of the same boundary structure [1, 23]. An example of Canny's capabilities is shown in figure 3.1.

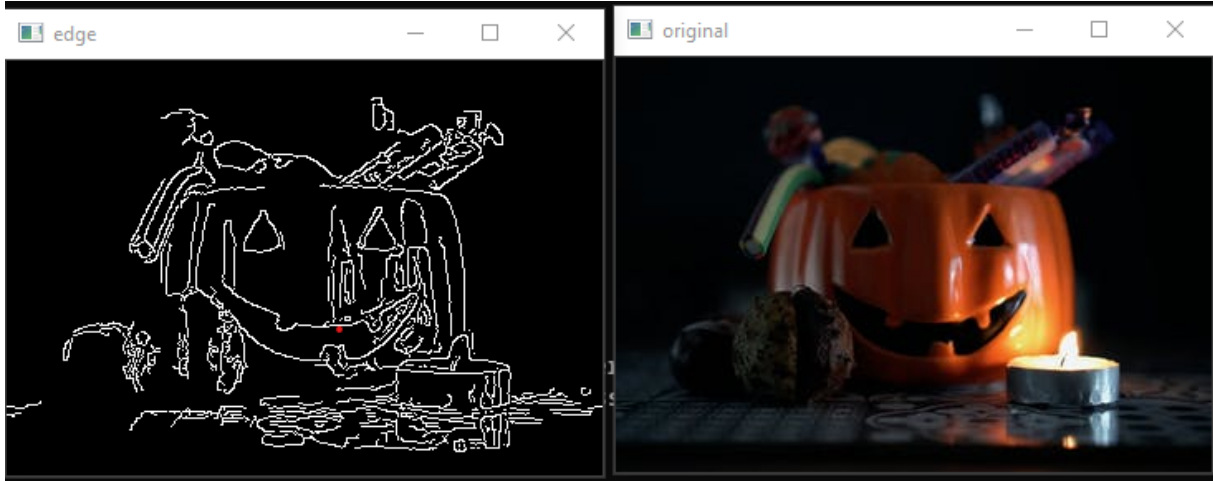


Figure 3.1: Example of a canny edge detection application [1]

In the context of this project, the Canny edge detection algorithm is employed to automatically identify the boundaries of a quadrilateral target by using the OpenCV contour approximation functions [24, 25]. By accurately detecting the corners and the centroid of the target, the algorithm provides the critical coordinates necessary for calibrating the AR camera lens. These coordinates form the basis for subsequent calibration steps such as central-shift correction, Field of View (FoV) adjustments, and compensation for lens distortion coefficients. The robustness of the Canny method against varying lighting conditions and noise makes it particularly effective for this application.

For more detailed explanations on the workings and implementation of the Canny edge detection algorithm in Python using OpenCV, readers are encouraged to consult the OpenCV tutorial [23] and the GeeksforGeeks guide [1]. These resources provide insights into the algorithm's multi-stage process and practical considerations in real-world applications.

The edge detection capabilities of OpenCV were used to provide the results shown in Figure 3.3.

This program enables the detection of the coordinates of the corners and the center of the target, as well as determining the length and width dimensions of the target.



Figure 3.2: Image taken with the camera with the target at the center

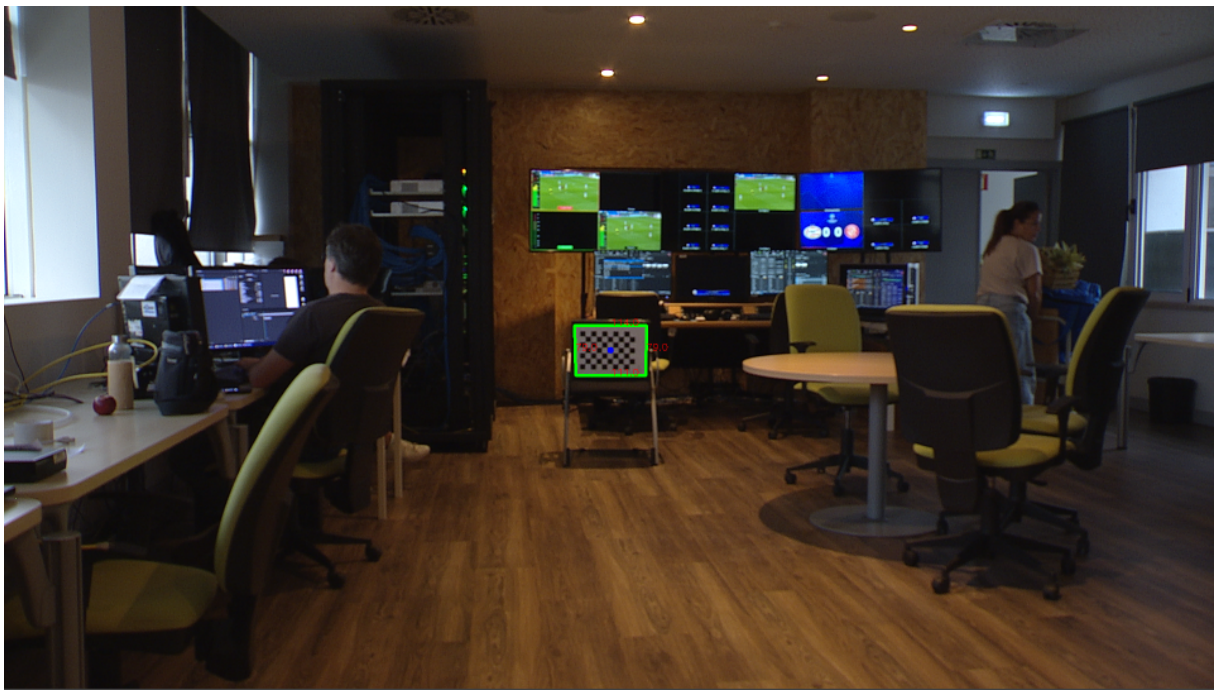


Figure 3.3: Edge detection program demonstration

In conclusion, this section has described the role of Canny edge detection in the project, emphasizing its utility in identifying the quadrilateral target's corners and centroid. The effective detection of these key points supports the calibration process, leading to more accurate adjustments in central-shift, FoV, and lens distortion parameters.

3.2 Using Blender for Testing

To evaluate the effectiveness of this program, multiple images from different angles and levels of distortion were needed. However, since the camera is not always available for this project, another program called "Blender" was used to simulate images that would resemble those provided by the real camera. Blender is a free and open-source 3D computer graphics software widely used for creating 3D models, animations, visual effects, and more. In this case, Blender was used to create a virtual camera and virtual targets.

This section outlines the workflow for setting up and rendering a scene in Blender, a widely used open-source 3D modeling and animation software. The following steps detail how to navigate the interface, adjust objects and camera settings, and produce a rendered image, as applied in this study. Blender was used in this project for simulating images for testing.

- 1. Loading a Scene:** Launch Blender and load the desired scene file to begin working with the 3D environment like in figure 3.4.

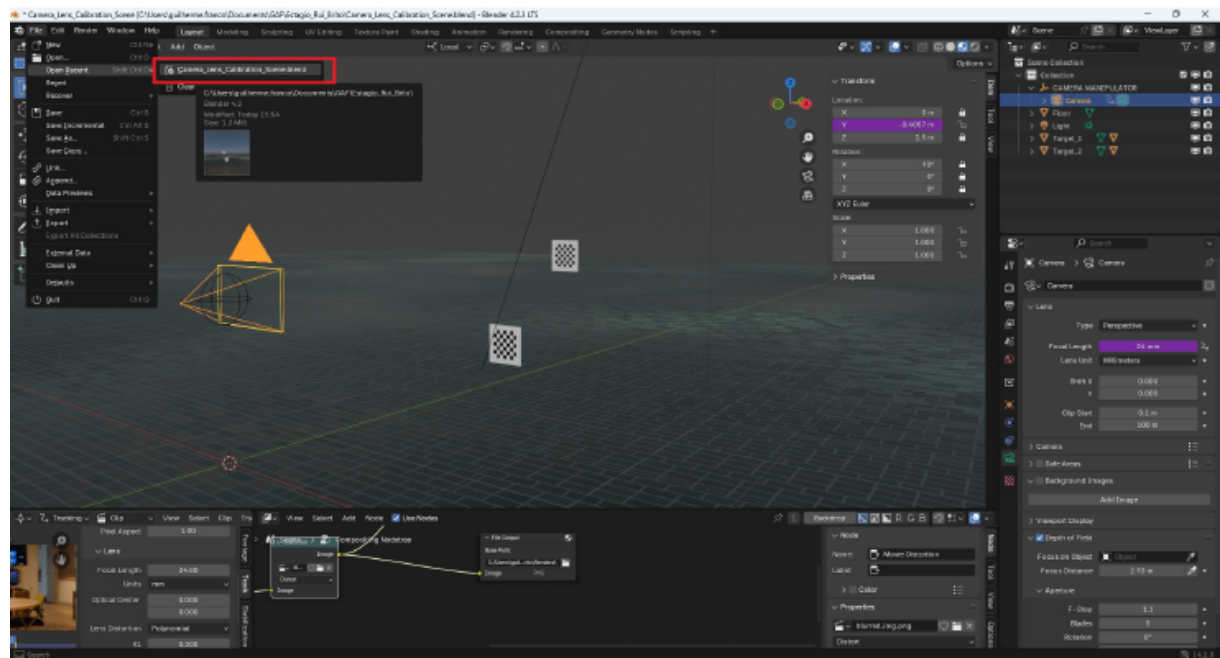


Figure 3.4: Loading a Scene

- 2. Viewport Navigation:** To explore the scene in the Viewport:

- Drag the middle mouse button (MMB) to rotate the view.
- Hold Shift and drag MMB to pan across the scene.

- Use the mouse wheel to zoom in or out.

3. Adjusting Object Positions: Select the target object (e.g., Target_1 or Target_2) from the right-hand menu. Modify its position and orientation by:

- Dragging the left mouse button (LMB) on the *Location* and *Rotation* fields.
- Typing specific values directly.
- Using the interface arrows for incremental adjustments.

Figure 3.5 illustrates this procedure.

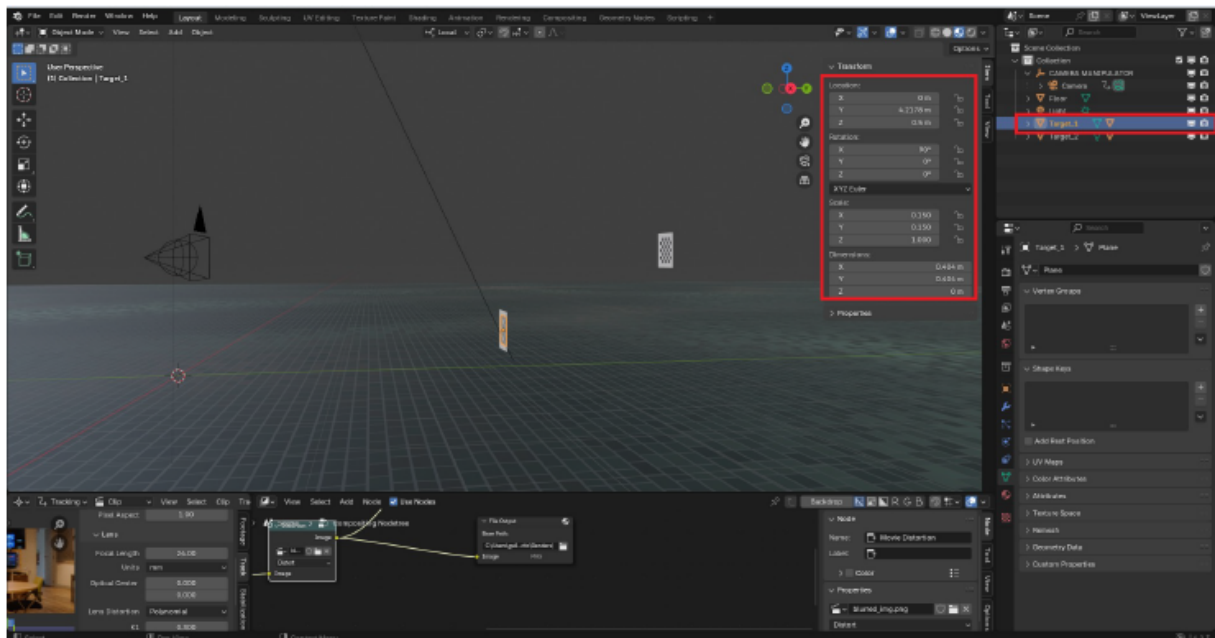


Figure 3.5: Adjusting Object Positions

- 4. Aligning the Viewport to the Camera:** To preview the camera's perspective, press Numpad-0 (the zero key on the numeric keypad).
- 5. Camera Positioning:** Select the CAMERA_MANIPULATOR object and adjust its *Location* and *Rotation* parameters, following the same method as for target objects.
- 6. Camera Lens Settings:** Select the child object Camera under CAMERA_MANIPULATOR, then access the *Data* sub-menu (indicated by a green camera icon in the bottom-right panel), figure 3.7. Adjust the following:
 - *Shift X / Shift Y*: Modify the center shift in the X and Y directions.
 - *Focus Distance*: Set the camera's focus point.

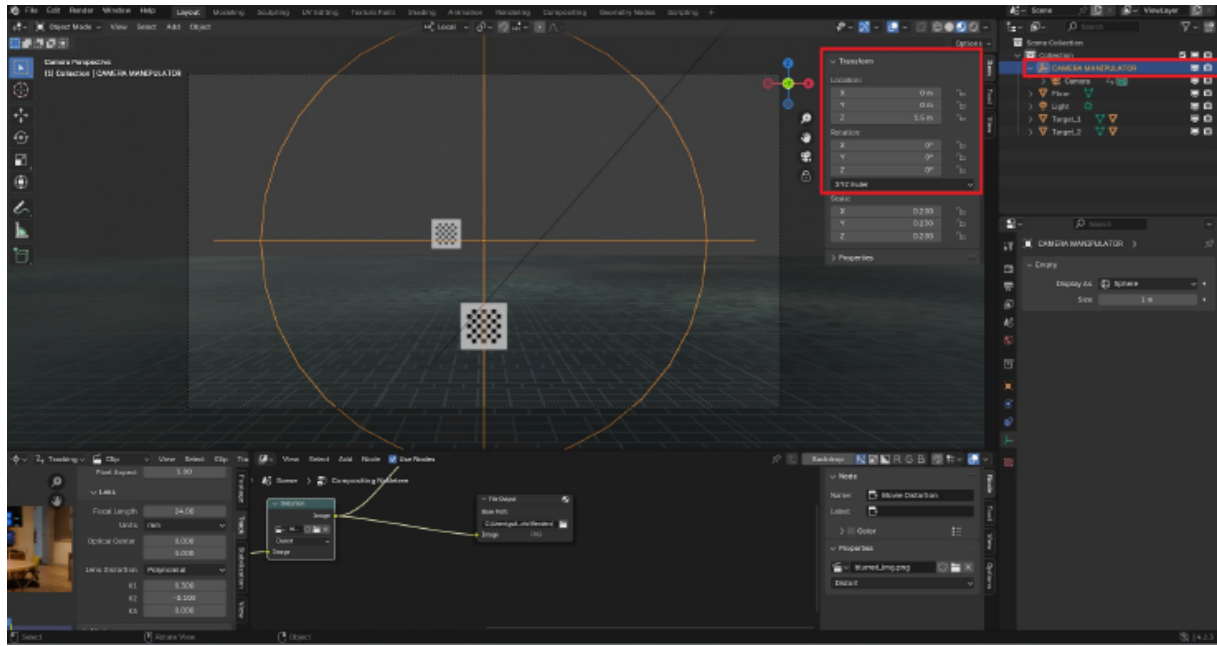


Figure 3.6: Camera Positioning

- *F-Stop*: Control depth of field; lower values increase blur for objects outside the focus distance, while higher values extend the in-focus range.
- *Focal Length*: Adjust this parameter (bottom-left corner) to change the field of view (FoV), reflected on the right-hand side.
- *K1 and K2*: Edit distortion coefficients directly below the *Focal Length*.
- *Nodal Offset*: Represented by the Y-value in the *Location* parameter (displayed in purple). Right-click and select *Edit Driver* to modify its governing function.

7. **Rendering the Image:** From the top-left menu, select *Render* → *Render Image* to initiate the rendering process, figure 3.8.
8. **Saving the Render:** In the rendering window, wait for the sample calculations to complete, then choose *Image* → *Save As...* to save the output, figure 3.9.
9. **Data Collection:** Currently, data extraction from the rendered image is performed manually. Automation of this process is feasible and could be implemented if deemed beneficial for future work.

This workflow demonstrates Blender's capability for precise scene manipulation and rendering, making it a valuable tool for 3D visualization in this research. To test the edge detection program,

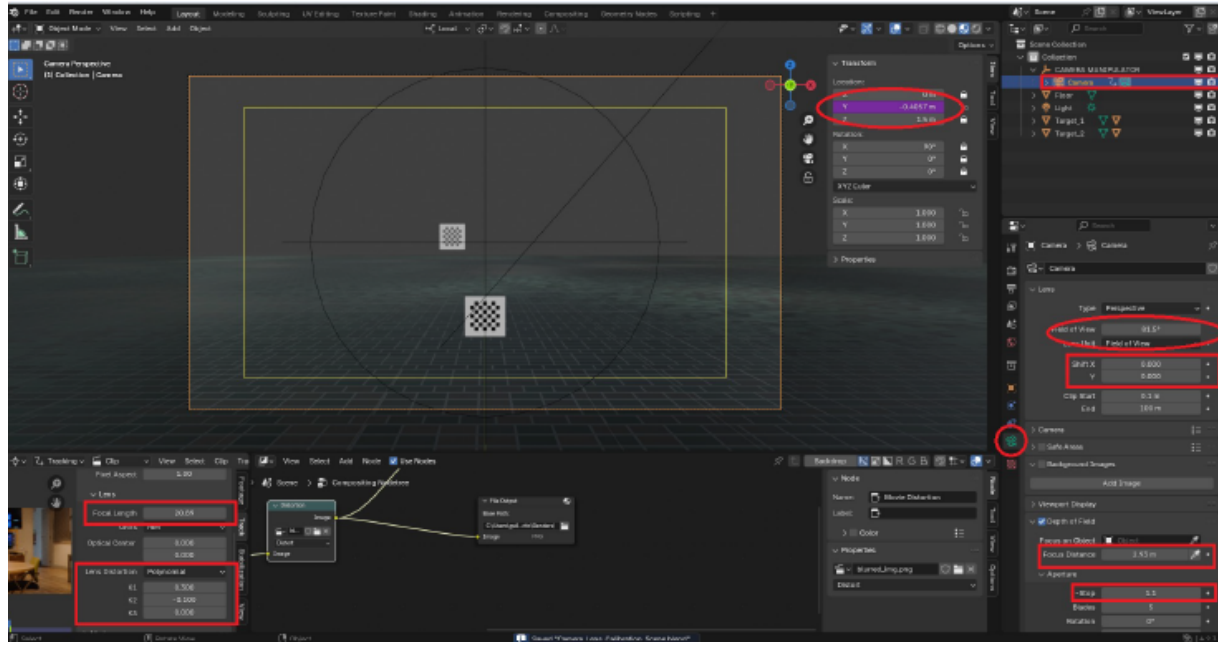


Figure 3.7: Camera Lens Settings

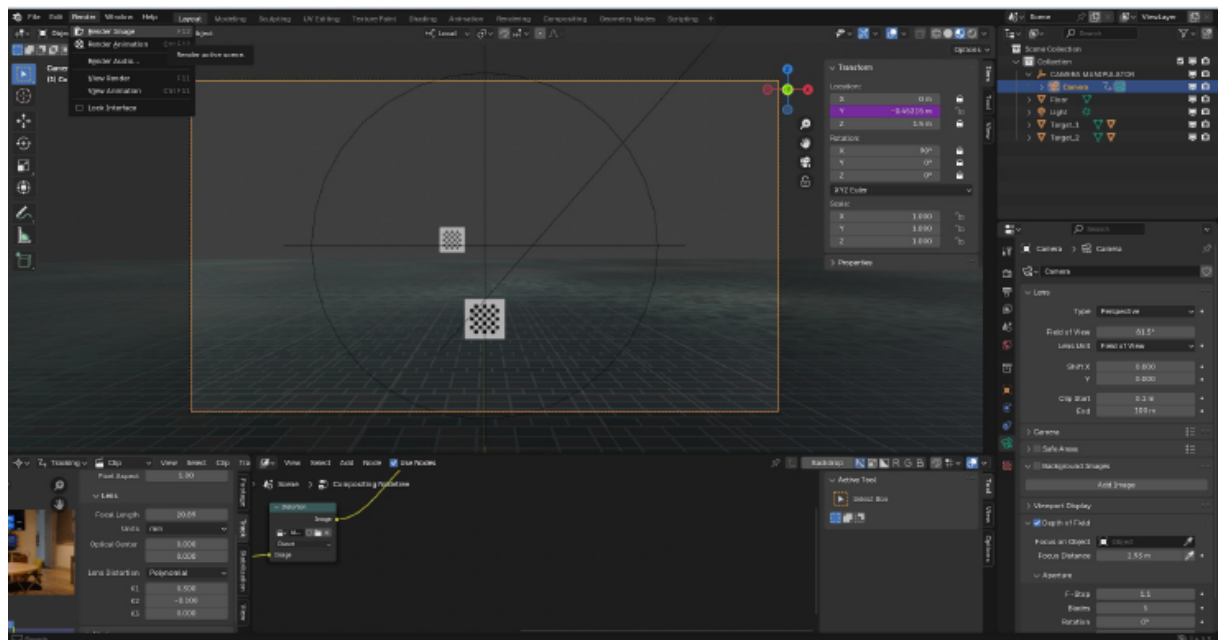


Figure 3.8: Rendering the Image

only one target was used. Multiple pictures from different angles and with varying distortions were taken and tested. Some of the results are shown in Figure 3.10.

From these tests, we can confirm that the program works as intended. Even for distorted images.

This method, however, presents certain limitations. When tested in real-world scenarios, the program occasionally misidentified the real target due to interference from ambient lighting. To

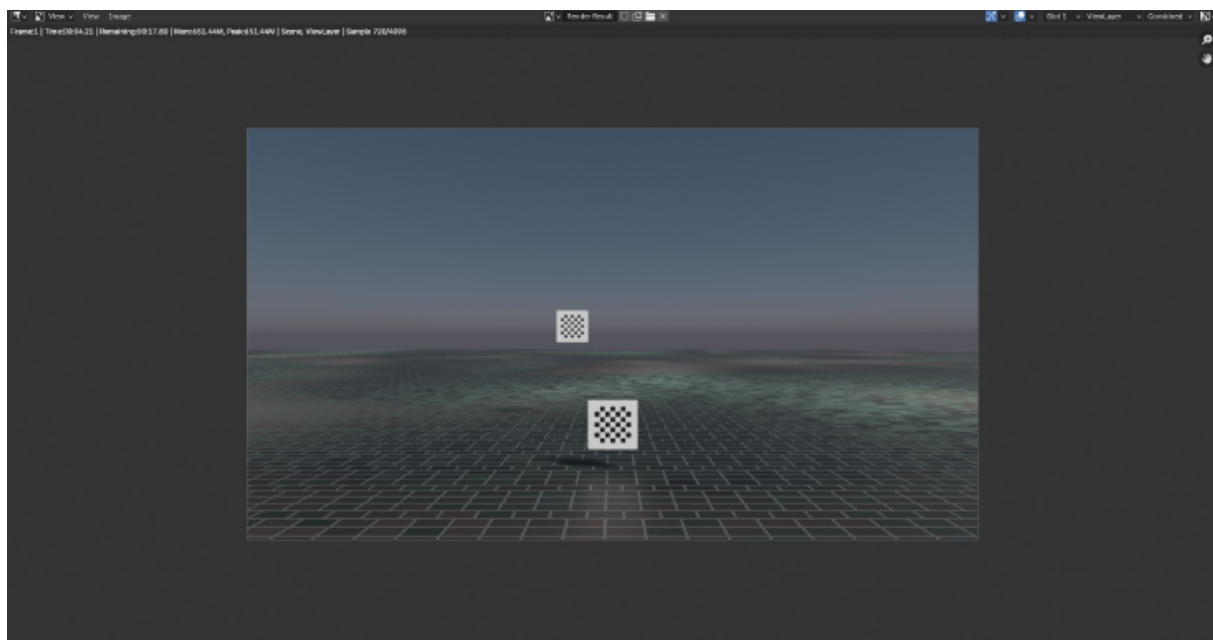
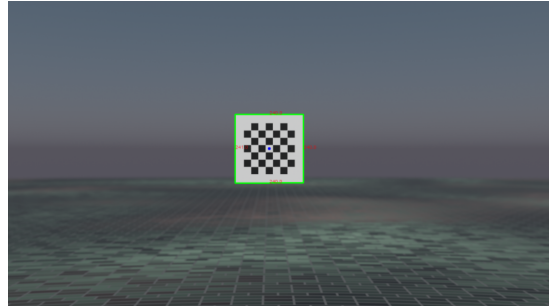
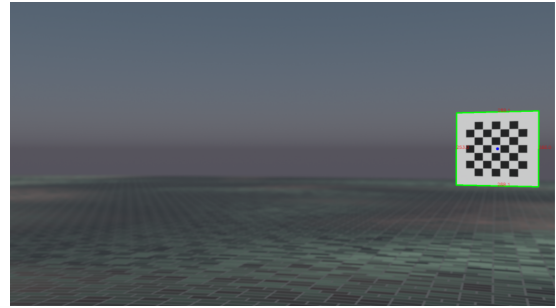


Figure 3.9: Saving the Render

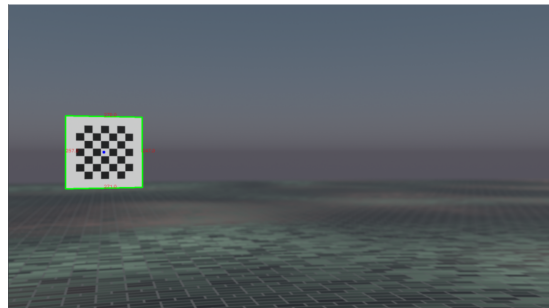
mitigate this issue, the target color was changed from white to red, as red is a less common color in real-world environments and contrasts well in studio settings that employ green screens.



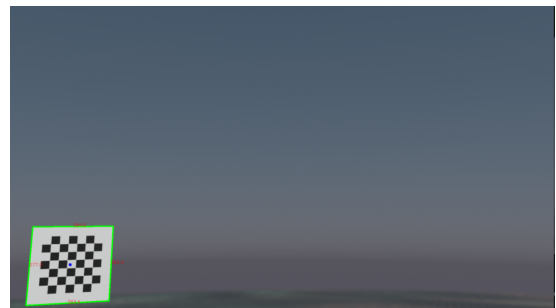
(a) Image 1



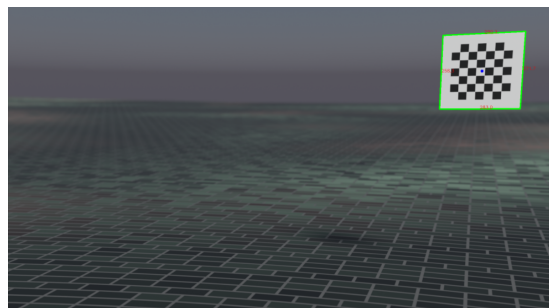
(b) Image 2



(c) Image 3



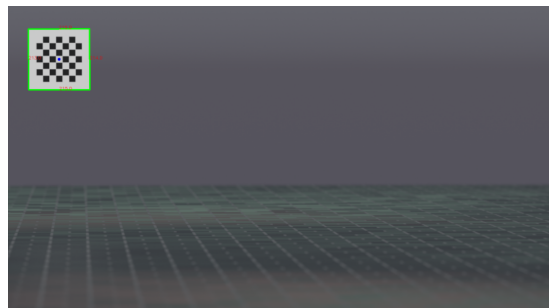
(d) Image 4



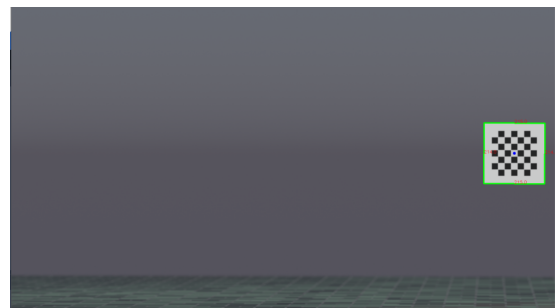
(e) Image 5



(f) Image 6



(g) Image 7



(h) Image 8

Figure 3.10: Edge Detection Results Visualization

Chapter 4

Camera Lens Calibration

A calibration algorithm that iteratively determines the distortion coefficient was developed. This chapter presents a detail explanation of how it worked. A summary of the results can be seen in Figure 4.5.

Virtual images were used for experimentation. These were created using R^3 software with known distortion coefficients. These images were recreated from the results of a previous calibration done manually at wTVision to ensure realistic values. The obtained images were saved in a folder. In this folder, there were images with different zoom and focus levels. For a specific zoom and focus level, for example Zoom 0 and Focus 0, there were four images, one for each distortion coefficient that needs to be determined: Center-shift¹, Field of View (**FoV**), K1 and K2.

The objective is to accurately determine the distortion coefficients of the (simulated) images. The distortion coefficients are then compared to the real values to evaluate the accuracy of the calibration process.

Before initiating the calibration process, it is essential to measure the dimensions and position of the real target. The origin of the real-world coordinate system is defined at floor level, directly below the camera's optical point. Using these measurements, a virtual object is inserted into the R^3 software. Additionally, the pan, roll, and tilt of the camera must all be set to zero.

¹Note that even though there is an image for calibrating the center-shift at each level, this is not necessary since for calibrating the center-shift only the zoom matters. In fact, only the images at zoom 0 and at maximum zoom are required. In other words, the same center-shift calibration results can be obtained using images captured at a zoom level of 0 with any focus value within its minimum and maximum range, and another image taken at the maximum zoom level with a focus value.

4.1 Center-shift calibration

A program capable of accurately detecting the corners of the target in the real world has been developed. In this step the R^3 software is used to incorporate a virtual object with the same pattern as the real-world target, using the image captured by the camera, to calibrate the center-shift.

At this stage, a virtual target with accurate dimensions is present in the virtual environment. The first step in the calibration process is determining the center-shift. Experimental validation of the existing calibration procedure has demonstrated that when the camera's tilt, pan, and roll are set to zero, the center-shift values correspond precisely to the pixel coordinates of the center of the light circle. This conclusion was derived through manual calibration of the center-shift and by using the edge detection program to identify the coordinates of the light circle's center.

The center-shift calibration procedure follows a systematic approach. Initially, the camera is set to its minimum zoom level, and the target is positioned at the center of the frame. The image is then focused, and the edge-detection program is utilized to determine the coordinates of the center point. These coordinates are subsequently updated as the new center-shift values. The camera zoom is then adjusted to its maximum level, and the target is refocused to verify the accuracy of the center-shift calibration.

The center-shift calibration process is illustrated in Figure 4.1. The real object is shown in Figure 4.1a, with the red square representing the target. In Figure 4.1b, a virtual cone is inserted into the R^3 software with an uncalibrated center-shift. The center coordinates of the real object are detected in Figure 4.1c, and the virtual cone is calibrated in Figure 4.1d. The final result is shown in Figure 4.2, with the virtual cone correctly calibrated to the real object. 4.2 shows the result of changing the pan, tilt and/or roll of an already calibrated center-shift.

4.2 K1, K2 and FoV calibration

Following this, the calibration of the FoV is performed. The procedure involves applying a pan movement to the camera, causing the target to shift laterally within the frame. The edge-detection program is then employed to extract the edges of the real target like shown in figure 4.3. Then the background is then turned off and the virtual object is inserted, for each iteration the program

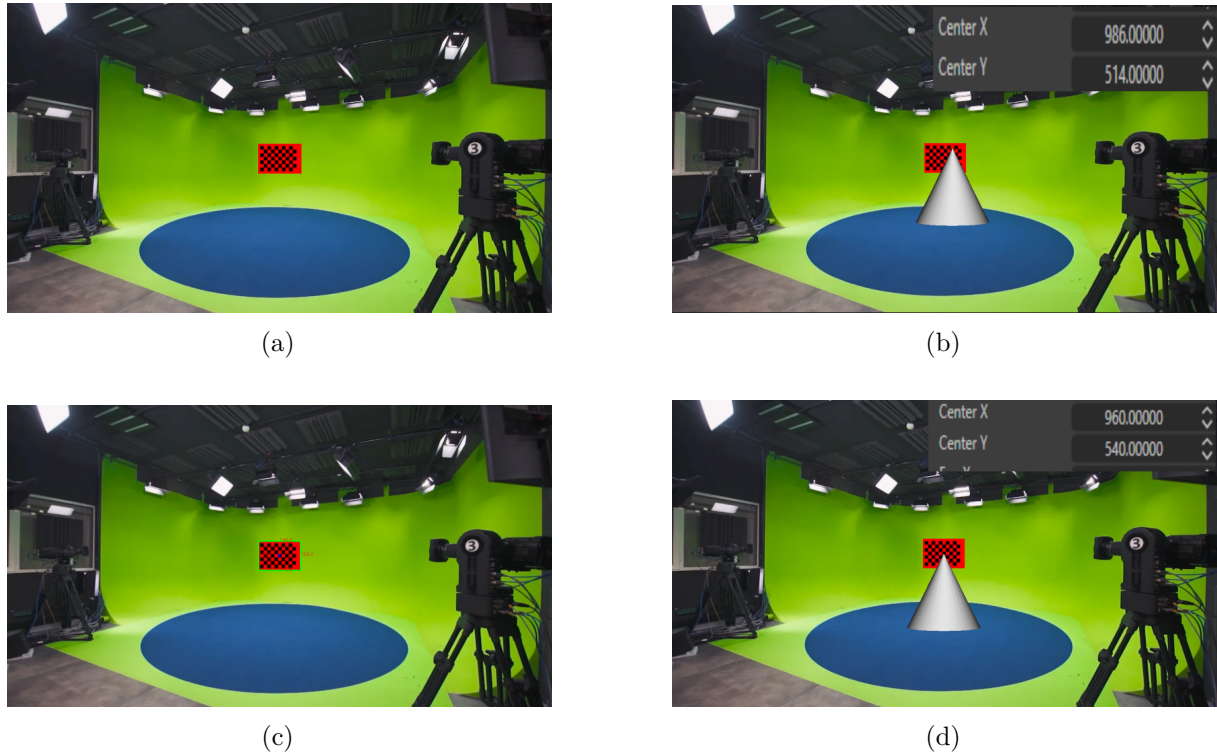


Figure 4.1: Example of a center-shift calibration:(a) - Real object (red square) at max zoom, (b) - Insertion of a virtual cone with uncalibrated center-shift, (c) - Detection real object center coordinates, (d) - Calibrated virtual cone.

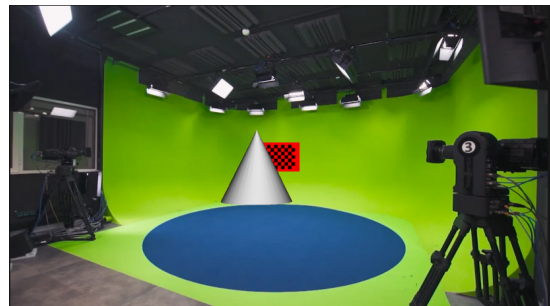


Figure 4.2: calibrated center-shift after changing the pan and tilt

detectes the corners of the virtual object² like shown in figure 9.13. It has been observed that the virtual object appears narrower than the real target. To achieve proper calibration, the FoV value must be adjusted until the virtual and real targets are perfectly aligned. This adjustment is conducted using a program to iteratively increment the FoV value until alignment is achieved. To optimize efficiency, the program employs a gradient descent function. A similar approach is utilized for the calibration of distortion parameters K_1 and K_2 .

A challenge encountered in this implementation was the misalignment of targets, even when their

²This means that the R^3 software has to take and save a snapshot for each iteration. These snapshots are saved and rewritten into the disk which constitutes a big limitations in terms of time efficiency.

widths were correctly calibrated. To address this, an improved approach was developed, which calculates the distance between the corner coordinates of the real and virtual objects. Calibration is considered complete when no corner exhibits a deviation beyond a predefined threshold. This method proves more effective than computing the total error across all corners, as summing individual errors does not provide an accurate representation of the alignment quality between the two targets.

After calibrating the K1 coefficient, determining the **FoV** value would possibly result in a misalignment of the targets. This was resolved by recalibrating the K1 coefficient after adjusting the **FoV** value multiple times until both values are correctly determined. This iterative process ensures that the calibration is accurate and that the targets are correctly aligned. The K2 coefficient is calibrated in a similar manner, with the K1 and K2 values being adjusted iteratively until both coefficients are correctly calibrated.

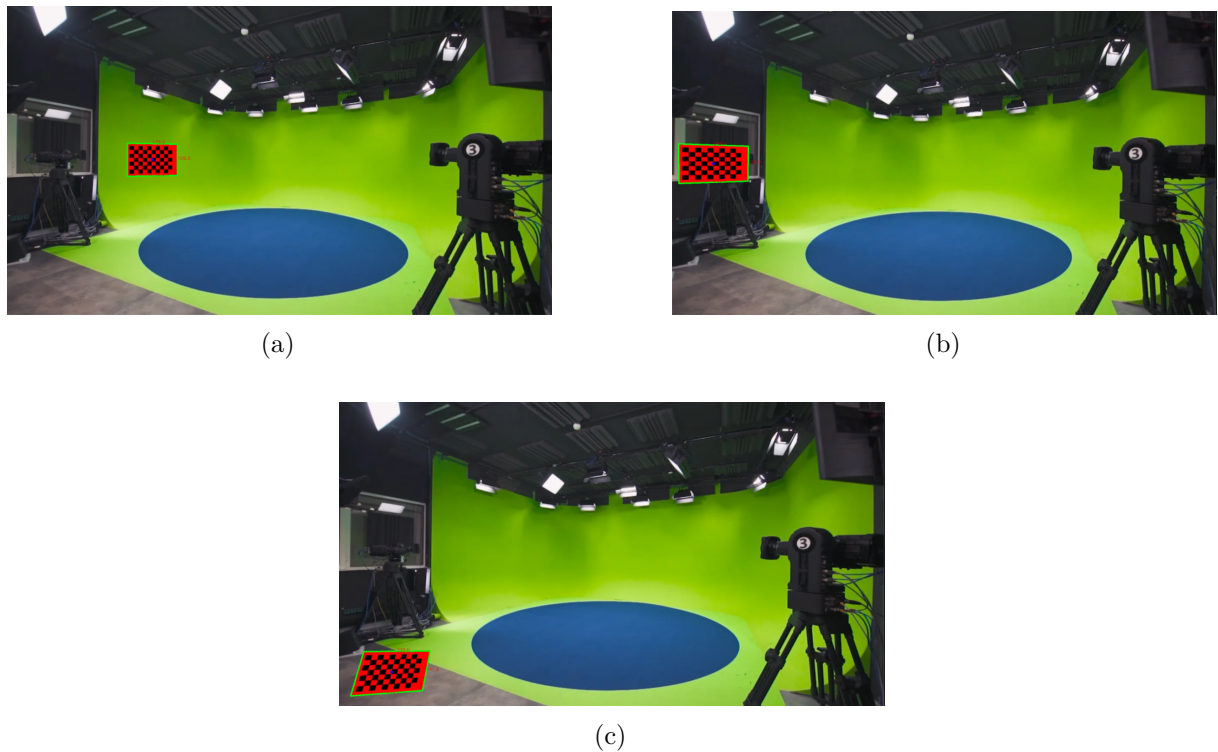


Figure 4.3: Example of K1, K2 and **FoV** calibration using edge detection to determine the real object corners coordinates: (a) - **FoV** calibration, (b) - K1 calibration, (c) - K2 calibration.

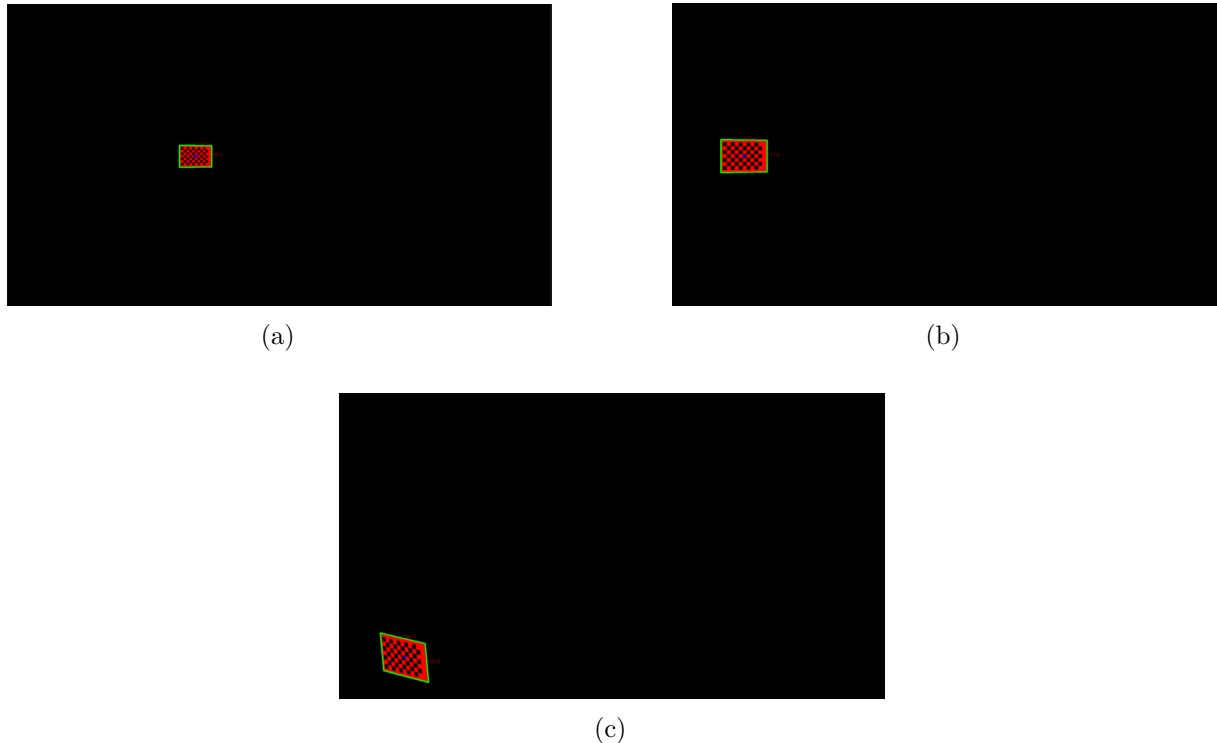


Figure 4.4: Example of K1, K2 and [FoV](#) calibration using edge detection to determine the virtual object corners coordinates: (a) - [FoV](#) calibration, (b) - K1 calibration, (c) - K2 calibration.

4.3 Calibration Scenarios

The calibration process using the algorithm follows the same principles as manual calibration. First, it calibrates the [FoV](#) to the best possible value. Then, it calibrates the K1 coefficient, iteratively refining both until they reach their optimal values. Afterward, the K2 calibration is performed using a similar iterative approach, adjusting both K1 and K2 until they are optimally calibrated.

After completing these steps, the algorithm's results could be categorized into three scenarios:

- **Scenario 1:** The [FoV](#) and K1 are correctly calibrated, and K2 is extremely close to 0. In this case, the effect of K2 is negligible. To optimize time efficiency, the algorithm is modified to stop if the K1 and [FoV](#) coefficients are already correctly calibrated. This is the most common scenario in real-world applications at most levels of calibration.
- **Scenario 2:** The K1 and [FoV](#) are not correctly determined, indicating that the K2 coefficient is not negligible. In this case, the algorithm proceeds to calibrate the K2 coefficient.

- **Scenario 3:** After calibrating the K2 coefficient, if the K1 and K2 coefficients are still not correctly calibrated, the algorithm may have become stuck, recalibrating to the same values repeatedly. To resolve this issue, the algorithm is modified to detect this scenario and forcibly adjust the K1 value before recalibrating K2 until both coefficients are correctly calibrated.

The program effectively determines the distortion coefficients with satisfactory accuracy. However, the calibration process is time-consuming, taking approximately 65 minutes to complete six levels, which is impractical for efficient operation. In the next chapter, we will explore strategies to optimize and reduce the calibration time.

4.4 Results

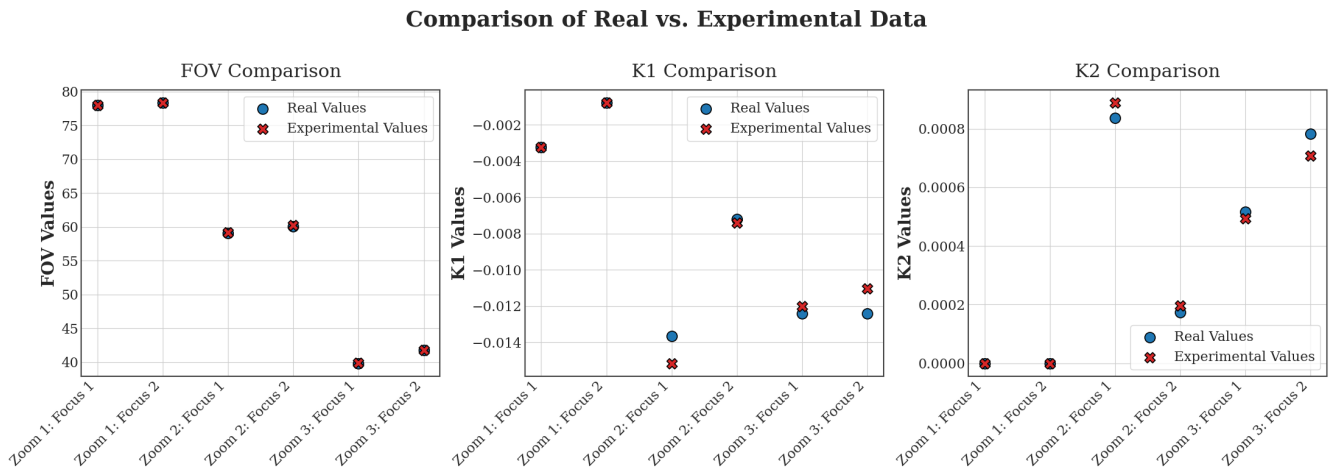


Figure 4.5: Distortion calibration results

Chapter 5

Optimizing Calibration Efficiency

This chapter explores strategies to reduce the calibration time of the algorithm. The initial approach involved transcribing the algorithm from Python to C++ to leverage the latter's greater computational efficiency. However, despite the significant development effort required, this optimization yielded only a marginal improvement, reducing calibration time by approximately 1%.

Given the limited success of this approach, an alternative solution was pursued. It was identified that the primary bottleneck in the program was the process of saving snapshots to the computer's disk during each iteration, which significantly slowed down execution. To address this, a virtual graphics card provided by wTVision was utilized, enabling direct communication with Python and allowing snapshots to be transferred in real-time instead of being stored on disk. This modification substantially improved the calibration efficiency.

5.1 MockBoard

The MockBoard is a virtual graphics card provided by wTVision that allows for the real-time transfer of images to the computer. This eliminates the need to save snapshots to disk, which significantly reduces the time required for calibration. The MockBoard is a software solution that emulates a video capture card, enabling the computer to receive video input directly from the R^3 software. This allows the computer to process the images in real-time, without the need to save snapshots to disk. The MockBoard is a proprietary software solution developed by wTVision, and is not available to the general public.

To use Mockboard in the calibration algorithm, the following steps are required:

1. Open the R^3 software in administrator mode.
2. Select MockBoard as the output in the R^3 software, like in figure 5.1.

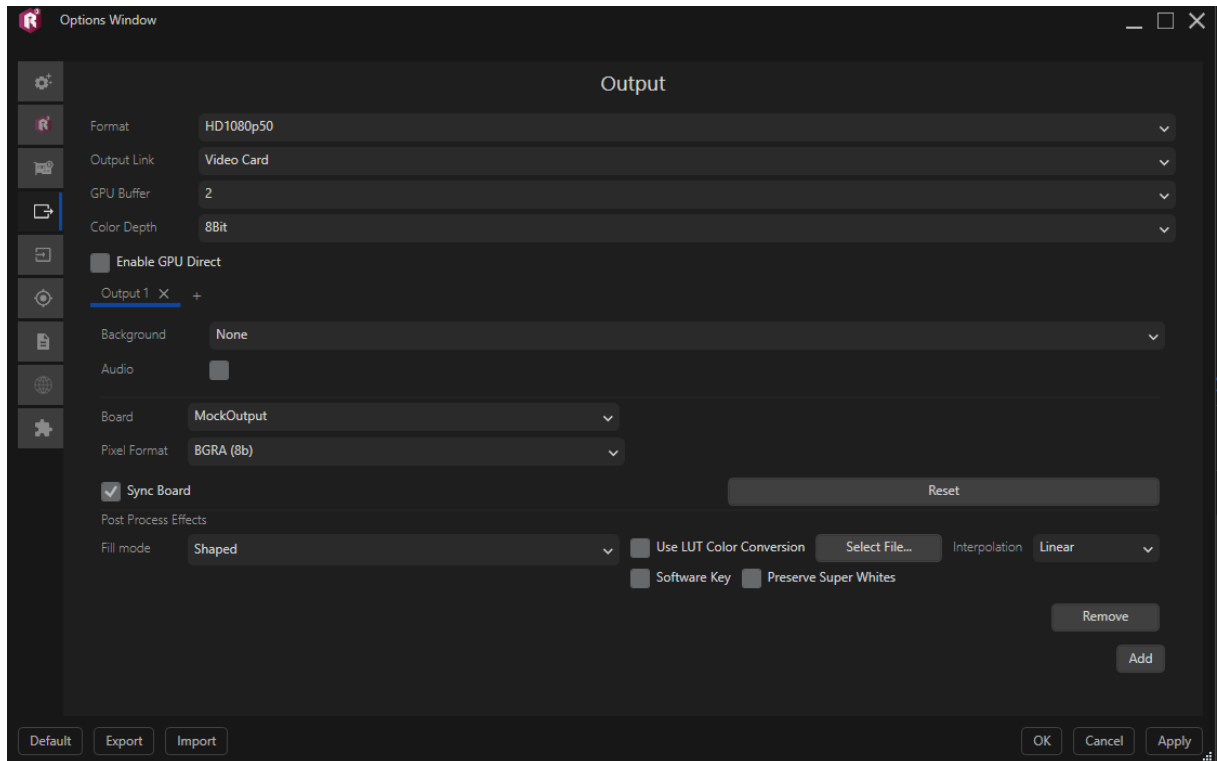


Figure 5.1: Selecting MockBoard as the output in the R^3 software.

5.1.1 Communication with MockBoard

The MockBoard functions as a local webapi with the following url:

```
"http://localhost:1987/api/v1/MockCard/MockOutput/GetImage"
```

Figure 5.2 illustrates its corresponding web page.

As demonstrated in figure 5.2, this url returns a string of an image in base64 format. To communicate with it using Python, http requests are used in order to return this string. The following steps outline how to establish communication between the Python script and the MockBoard:

1. First, the correct headers need to be added. This can be achieved by using the following

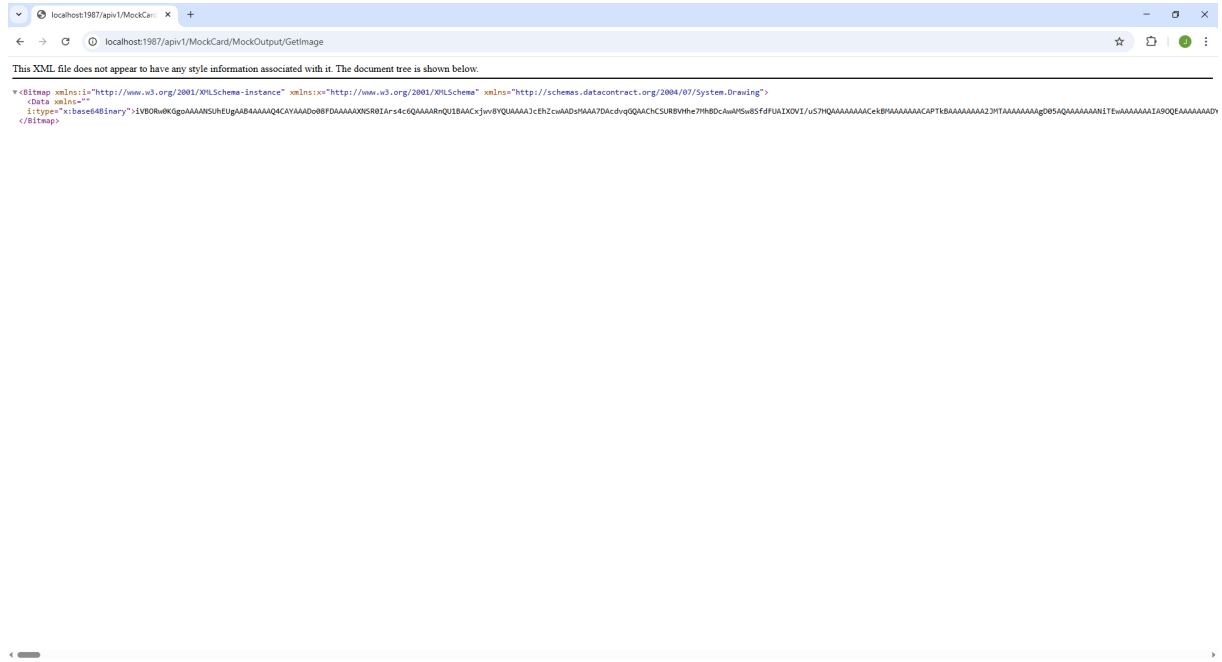


Figure 5.2: MockBoard web page.

code:

```
response = requests.get(url, headers=headers)
```

These headers are displayed in Table 9.1 in the annex chapter 9.

2. Using HTTP requests it is possible to obtain the image in base64 format.
3. The base64 image is then converted into a png image using the base64 and BytesIO Python libraries.

Using the MockBoard, it takes exactly 0.015 seconds to obtain an image, which is a significant improvement over the previous method of saving snapshots to disk, which took around 0.3 seconds. This improvement should reduce the algorithm's calibration time by at least 90%.

5.2 Results

The calibration algorithm was tested using the MockBoard to evaluate the impact on calibration time. The results are presented in figure 5.3.

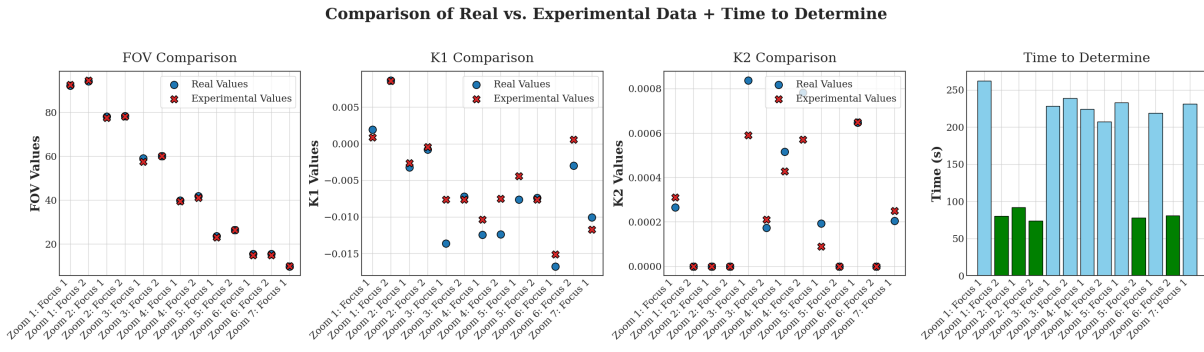


Figure 5.3: Distortion calibration results using the MockBoard.

As shown in figure 5.3, the calibration time was significantly reduced, only taking 35.1 minutes to calibrate 13 levels of zoom/focus, using the old method would've taken above 120 minutes. This significant improvement in efficiency demonstrates the potential of the MockBoard to optimize the calibration algorithm.

As expected, when K2 is 0 it takes less time to calibrate. The green bars in figure 5.3 represent the time taken to calibrate when K2 is 0, while the blue bars represent the time taken to calibrate when K2 is not 0.

A subjective evaluation of a sample calibration result is presented in figure 5.4. Additional calibration levels are provided in the annex section.

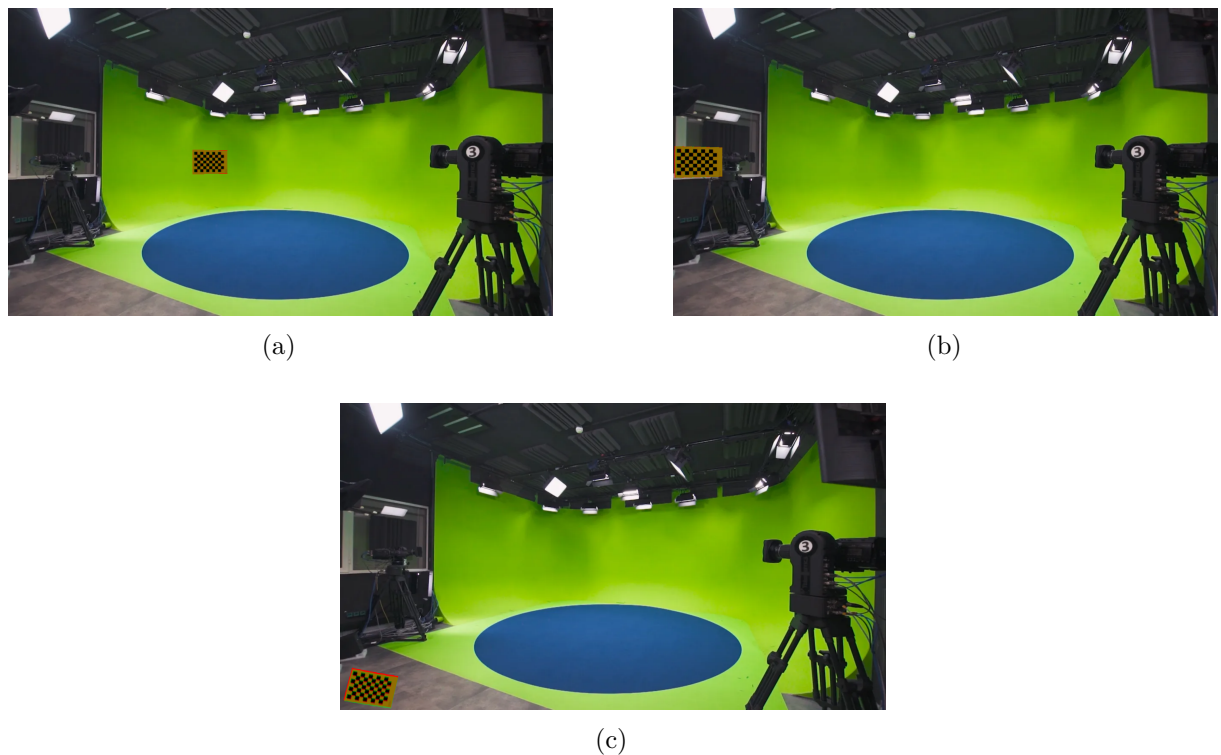


Figure 5.4: Zoom 1 Focus 1 - (a) FoV, (b) K1, (c) K2.

Chapter 6

Image Deblurring Using Neural Networks

In real-world applications, images are frequently degraded by blur, most commonly due to defocus. For the camera calibration algorithm to function effectively, a minimum level of image quality is required in order to accurately estimate camera parameters. To enhance image quality and meet this requirement, image deblurring techniques can be employed. This chapter presents an overview of the deblurring approach explored in this work, with a focus on its implementation using neural networks.

Due to constraints in research time and computational resources, the current implementation did not achieve satisfactory deblurring performance. Nevertheless, the development process offers valuable insights and establishes a foundation that may inform and support future research efforts in this area.

6.1 Dataset

The dataset used for training the neural network is a set of blurred images and their corresponding sharp images. These images were obtained using blender, since its able to recreate accurate images of an out-of-focus camera. Using a python script generated 500 set of blurred and the corresponding sharp images. Each image consists of a red chessboard square with random size, position and aspect ratio with a random studio in the background.

6.2 Deblurring using EDSR

For the deblurring task, we used the Enhanced Deep Super-Resolution (EDSR) network, originally designed for single-image super-resolution. Although EDSR was developed to upscale low-resolution images to high-resolution outputs, it has been shown to be effective for image restoration tasks such as deblurring.

EDSR is a deep convolutional neural network that removes unnecessary modules, such as batch normalization layers, from its predecessor models (e.g., SRResNet) to improve performance. It consists of multiple residual blocks without downsampling, enabling the network to maintain spatial information and focus on learning fine details.

In our case, the input to the EDSR network is a blurred image, and the output is its deblurred (sharpened) version. The network is trained to minimize the pixel-wise loss between the predicted deblurred image and the ground truth sharp image.

Due to limitations in computational resources, the training images were downsampled from 1080p to 720p resolution. However, this reduction in resolution may have had a detrimental impact on performance, as it introduced an additional layer of degradation. Since the input images were already blurred, further downscaling likely compounded the loss of high-frequency details, making the deblurring task more challenging for the neural network.

6.3 Loss Function

6.3.1 MSELoss

The MSELoss function was the first to be tested for image deblurring. The training process was made to prioritize the deblurring of the chessboard square, which is the primary region of interest, while assigning less importance to the surrounding areas.

This approach involves recording the coordinates of the chessboard corners in the training dataset and applying a crop to both the blurred and sharp images to isolate the relevant region. The algorithm is then trained using the Mean Squared Error Loss (MSELoss) function, with a weighted focus on the chessboard square.

Specifically, the MSELoss for the chessboard region is computed and weighted by a factor of 0.9,

while the loss for the remaining parts of the image is weighted by 0.1. The final loss is calculated as the weighted sum of these two components:

$$\mathcal{L}_{\text{total}} = 0.9 \cdot \mathcal{L}_{\text{chessboard}} + 0.1 \cdot \mathcal{L}_{\text{background}} \quad (6.1)$$

MSELoss alone proved to be suboptimal for effective image deblurring. As a result, additional loss functions were explored in subsequent experiments.

6.3.2 The Structural Similarity Index ([SSIM](#))

The Structural Similarity Index Measure ([SSIM](#)) was subsequently evaluated as an alternative loss function. SSIM is designed to model the perceptual similarity between images by considering luminance, contrast, and structural information, making it more aligned with human visual perception compared to pixel-wise metrics such as MSE.

Despite its theoretical advantages, the use of SSIM as the sole loss function did not yield satisfactory deblurring results in this implementation. One possible reason is that SSIM, while effective in preserving perceptual quality, may not provide sufficient gradient signals for restoring fine image details in severely blurred regions—especially when used without additional complementary losses.

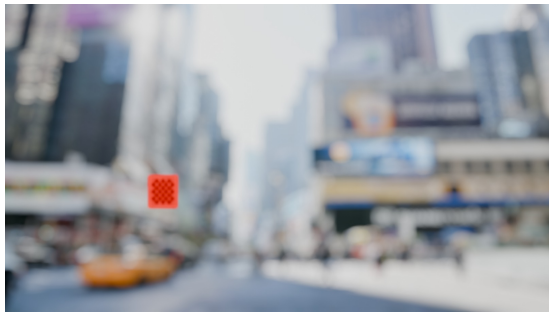
These findings suggest that more advanced or hybrid loss formulations may be necessary to achieve robust deblurring performance, such as combining SSIM with MSE, perceptual loss, or adversarial objectives.

6.4 Mask Implementation

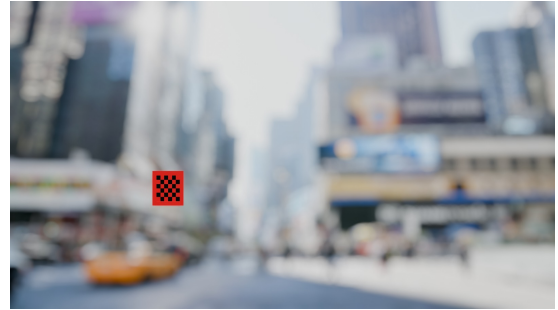
Given the limited effectiveness of the deblurring algorithm, an alternative approach was adopted to enable the calibration algorithm to function with slightly blurred images.

Leveraging OpenCV’s image processing capabilities, the checkerboard pattern can still be detected reliably, provided the image is not excessively blurred. Based on this detection, the red checkerboard region is identified, and a binary mask is applied to isolate this region from the background.

This masking approach proved to be a practical solution for camera calibration, as it allowed the algorithm to focus on the region of interest despite minor image degradation. However, minor inaccuracies were observed in the estimated position and size of the masked checkerboard. These deviations may introduce slight errors in the calibration results and warrant further refinement of the detection and masking process. A result from this process is in figure 6.1.



(a) Original input image without masking.



(b) Masked image with the red checkerboard region isolated.

Figure 6.1: Comparison between the original image and the masked result used for calibration.

Chapter 7

Deep Learning-Based Estimation of k_1 and k_2

Conventional camera calibration techniques, such as those based on the R^3 method, typically require controlled environments, structured scenes, and the presence of a known target—such as a planar checkerboard pattern. These constraints significantly limit their applicability in real-time, large-scale, or field-based scenarios.

To overcome these limitations and improve calibration efficiency, a deep learning-based approach was developed to estimate the radial distortion coefficients k_1 and k_2 directly from a single distorted image. This method eliminates the need for calibration targets by training a convolutional neural network (CNN) on synthetically generated images, each labeled with known distortion parameters computed via the Brown–Conrady model.

Evaluation on test data demonstrated the effectiveness of the model: predicted k_1 values exhibited errors below 5%, while k_2 estimates were typically within 10% of their ground truth values. These results underscore the method’s potential as a fast and practical alternative to traditional calibration pipelines, particularly in unconstrained or dynamically changing environments.

7.1 Synthetic Dataset Generation

To train the deep learning model for distortion estimation, a synthetic dataset comprising 5000 images was created using physically accurate radial distortion models. Each image was paired with the ground truth distortion parameters used to generate it, allowing supervised regression.

This follows established practices in learning-based camera calibration [8, 9, 26].

7.1.1 Source Images

Undistorted base images were sampled from the Places365 dataset, a large-scale natural scene benchmark widely used in computer vision tasks [27]. Each image was resized to a fixed resolution of 256×256 pixels, ensuring consistent image dimensions and facilitating efficient batch training.

7.1.2 Distortion Simulation

Radial distortion was applied according to the Brown–Conrady model [6], which simulates the physical displacement of light rays due to nonlinear refraction in real lenses. The distorted coordinates (x_d, y_d) were computed from the undistorted coordinates (x, y) as:

$$\begin{aligned} x_d &= x \left(1 + k_1 r^2 + k_2 r^4 \right), \\ y_d &= y \left(1 + k_1 r^2 + k_2 r^4 \right), \end{aligned} \tag{7.1}$$

where $r = \sqrt{x^2 + y^2}$ is the radial distance from the optical center. This formulation closely models real optical systems, particularly those exhibiting third- and fifth-order radial distortion.

The distortion coefficients were randomly sampled from physically plausible ranges observed in consumer-grade and wide-angle lenses:

$$k_1 \sim \mathcal{U}(-0.4, 0.4), \quad k_2 \sim \mathcal{U}(-0.2, 0.2). \tag{7.2}$$

7.1.3 Supervision Labels

Each synthetically distorted image was paired with its corresponding ground truth parameters (k_1, k_2) , which served as regression targets during training. The network was optimized using the mean squared error (MSE) loss function, defined as:

$$\mathcal{L}_{\text{MSE}} = \frac{1}{2} \left[(k_1^{\text{pred}} - k_1^{\text{true}})^2 + (k_2^{\text{pred}} - k_2^{\text{true}})^2 \right]. \tag{7.3}$$

This loss penalizes deviations between predicted and true distortion coefficients and encourages stable convergence.

7.1.4 Training Process

To monitor convergence, the model was trained over multiple epochs while recording the average MSE loss at each epoch. The evolution of the loss function is shown in Figure 7.1.

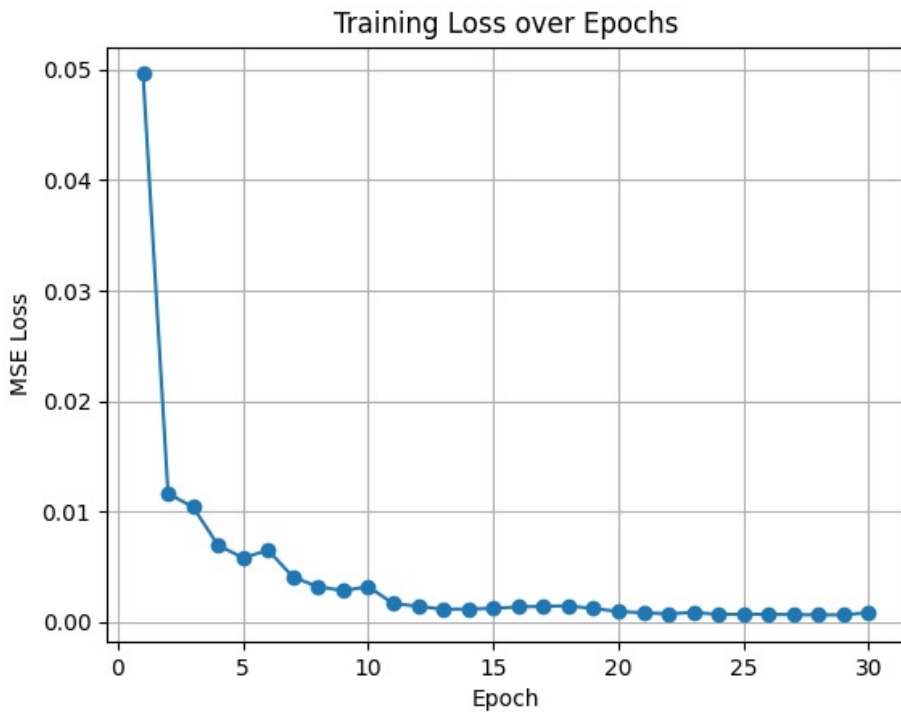


Figure 7.1: Training loss (MSE) per epoch.

As shown in the loss curve, the model undergoes rapid improvement during the initial epochs, with the loss decreasing significantly up to approximately 15 epochs. Beyond this point, the loss curve plateaus, indicating convergence. Consequently, a training schedule of 20–30 epochs was selected to ensure convergence while minimizing the risk of overfitting.

7.1.5 Results

A convolutional neural network based on the ResNet-18 architecture [10] was trained to regress the distortion coefficients k_1 and k_2 from synthetically distorted images. After training for 30 epochs using the MSE loss function, the model was evaluated on unseen test samples.

Figure 7.2 shows a representative result from the test set, comparing the input distorted image with the corresponding rectified output generated using the predicted distortion parameters. The visual quality of the rectified result confirms that the model effectively recovers plausible distortion coefficients capable of correcting significant radial warping.

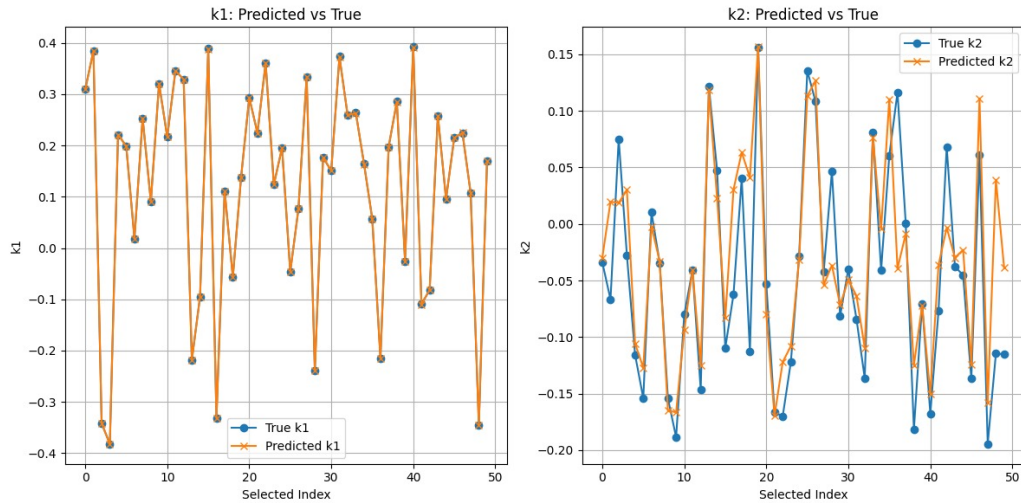


Figure 7.2: Distorted input (left) and rectified output (right) using predicted k_1 and k_2 . The CNN effectively compensates for radial distortion.

Quantitatively, the model achieved mean relative errors below 5% for k_1 and typically under 10% for k_2 . These results demonstrate the model's suitability for single-image camera calibration in cases where conventional multi-image or pattern-based methods are impractical.

Chapter 8

Conclusions and Future Work

This thesis presented the development of an automated camera lens calibration algorithm aimed at improving the efficiency and accuracy of calibration procedures for augmented reality (AR) applications, particularly in the context of wTVision’s broadcasting technologies. The proposed system addressed the key limitations of existing manual methods, which are both time-consuming and heavily dependent on operator expertise.

The developed calibration algorithm introduced a systematic approach for estimating distortion coefficients, including center-shift, field of view (FoV), and radial distortion parameters (K1 and K2), using image processing techniques such as Canny edge detection. The use of Blender for synthetic data generation and the R3 software allowed controlled experimentation under realistic AR scenarios. The algorithm achieved distortion coefficient estimations with a relative error below the 5% target for most scenarios, thus meeting the accuracy goals set at the outset.

A significant contribution of this work was the implementation of the MockBoard interface, which allowed real-time image acquisition without writing snapshots to disk. This drastically reduced calibration time from over 120 minutes to approximately 35 minutes for 13 zoom/focus levels—achieving over a 70% reduction in runtime.

The thesis also explored a complementary research path in image deblurring using convolutional neural networks. Although the results were not satisfactory due to research time and computational limitations, the work lays the groundwork for future studies by evaluating architectures like EDSR and experimenting with loss functions such as MSE and SSIM. Additionally, an effective workaround using OpenCV masking was introduced, enabling the calibration process to function even with mildly blurred images.

Future Work

- **Real-Time Calibration:** Further development could focus on real-time calibration directly from live video streams, allowing dynamic adjustment during live broadcasts.
- **Deep Learning for Deblurring:** Future research may revisit the use of neural networks for image restoration, leveraging larger datasets, higher resolutions, and more powerful hardware. Hybrid loss functions and generative approaches such as GANs could be explored.
- **Full Automation and UI Integration:** Integrating the calibration system into a user-friendly graphical interface and fully automating parameter selection would further reduce operator dependency.

In summary, this project successfully demonstrated the potential for automating camera lens calibration using computer vision and software engineering techniques. It significantly reduced calibration time while maintaining accuracy, paving the way for more scalable and efficient AR workflows in professional broadcasting environments.

Chapter 9

Annexs

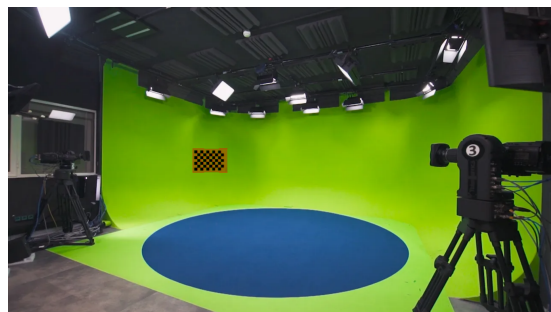
9.1 HTTP Headers

Table 9.1: HTTP Headers Used in the Request

Header	Value
Accept	text/html, application/xhtml+xml, application/xml;q=0.9, image/avif, image/webp, image/apng, */*;q=0.8, application/signed-exchange;v=b3;q=0.7
Accept-Encoding	gzip, deflate, br, zstd
Accept-Language	pt-PT, pt;q=0.9, en-US;q=0.8, en;q=0.7
Cache-Control	max-age=0
Connection	keep-alive
Host	localhost:1987
Sec-Fetch-Dest	document
Sec-Fetch-Mode	navigate
Sec-Fetch-Site	none
Sec-Fetch-User	?1
Upgrade-Insecure-Requests	1
User-Agent	Mozilla/5.0 (Windows NT 10.0; Win64; x64) AppleWebKit/537.36 (KHTML, like Gecko) Chrome/133.0.0.0 Safari/537.36
sec-ch-ua	"Not(A:Brand";v="99", "Google Chrome";v="133", "Chromium";v="133")

Header	Value
sec-ch-ua-mobile	?0
sec-ch-ua-platform	"Windows"

9.2 Calibration Results



(a)



(b)



(c)

Figure 9.1: Zoom 1 Focus 1 - (a) FoV, (b) K1, (c) K2.

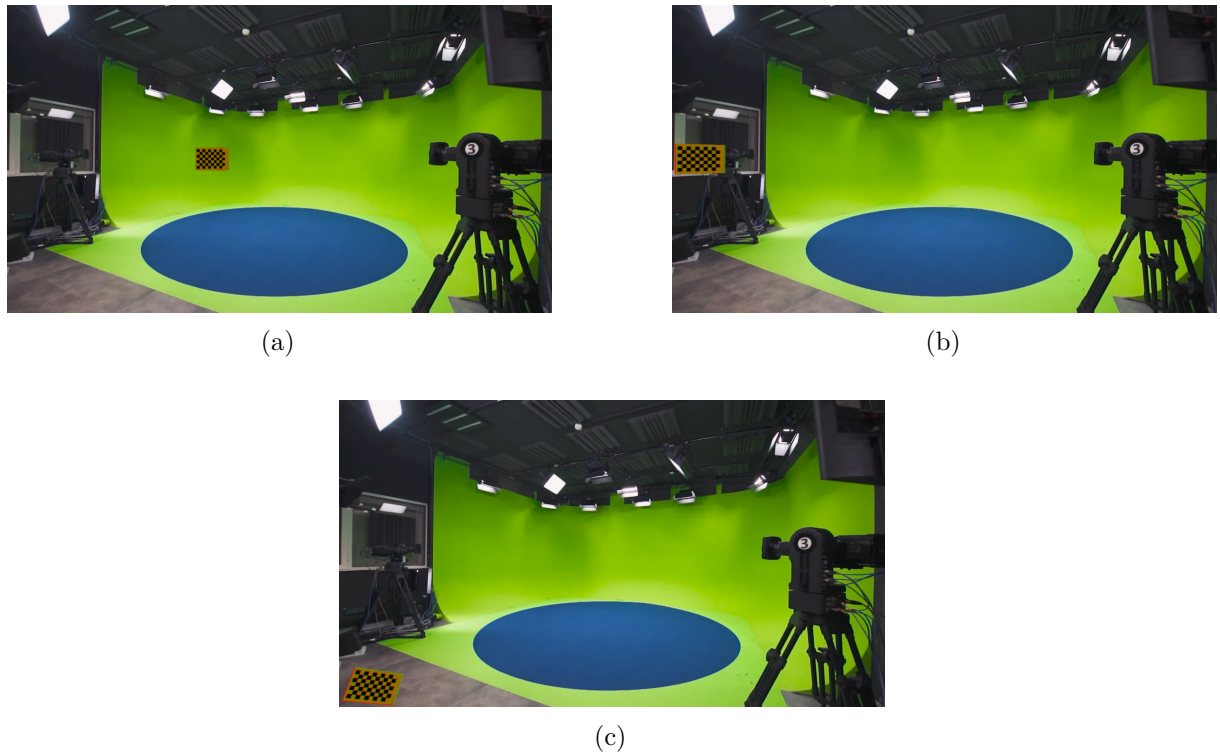


Figure 9.2: Zoom 1 Focus 2 - (a) FoV, (b) K1, (c) K2.

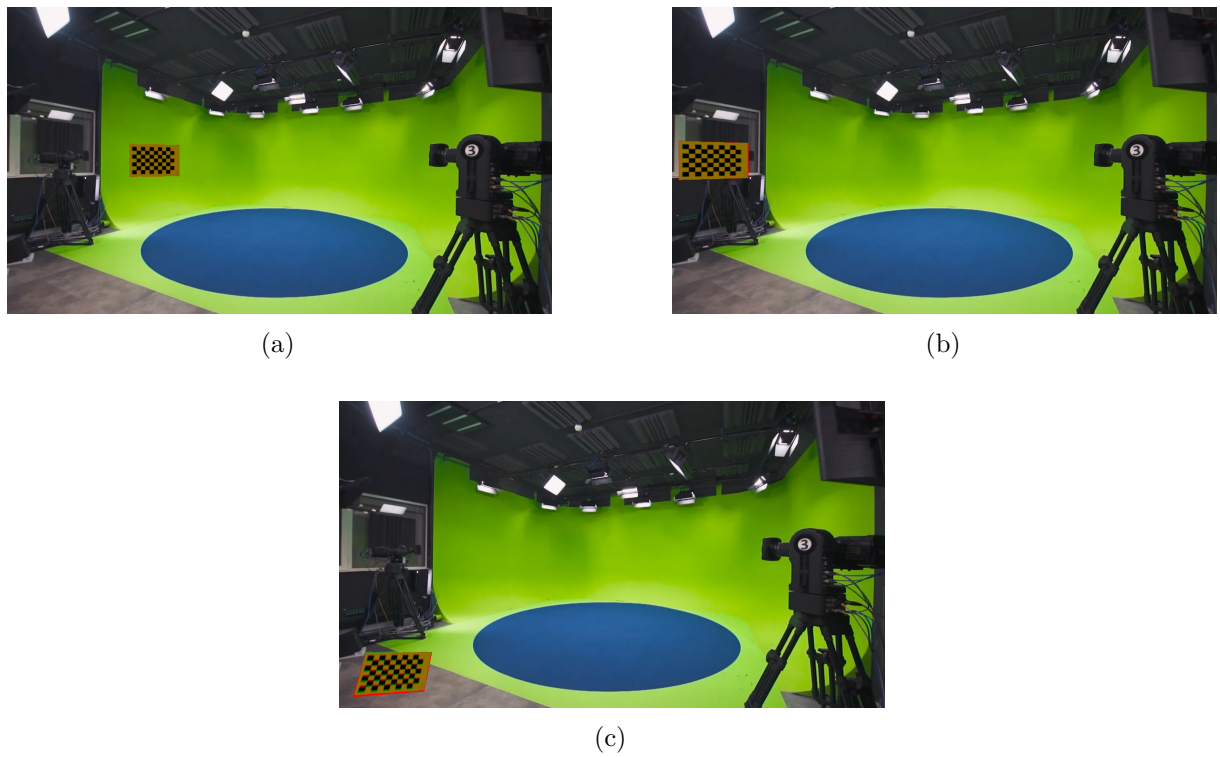


Figure 9.3: Zoom 2 Focus 1 - (a) FoV, (b) K1, (c) K2.

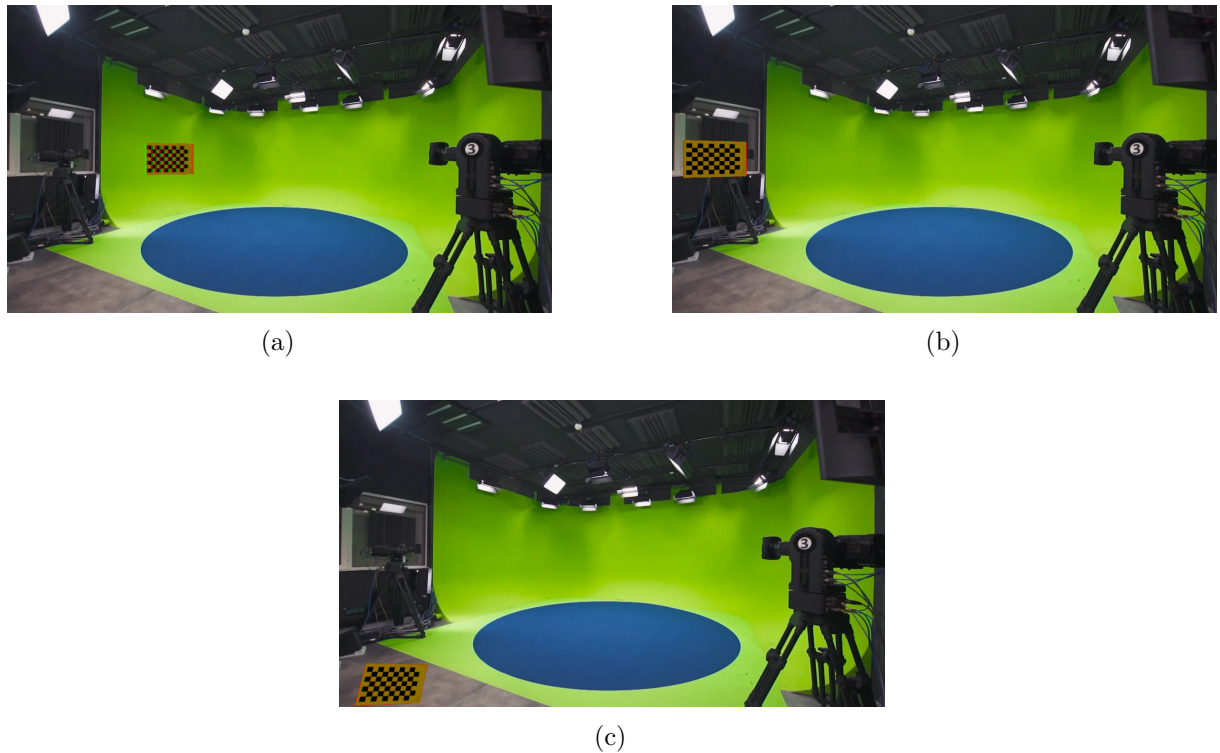


Figure 9.4: Zoom 2 Focus 2 - (a) FoV, (b) K1, (c) K2.

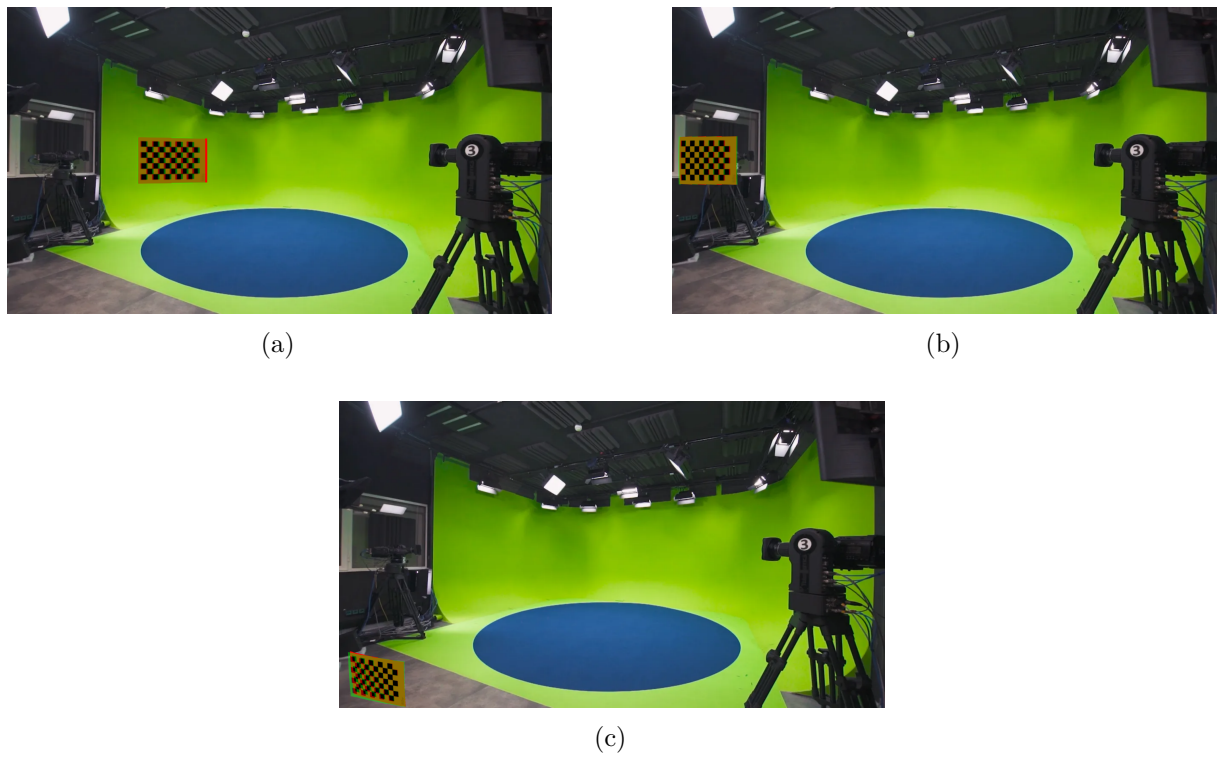


Figure 9.5: Zoom 3 Focus 1 - (a) FoV, (b) K1, (c) K2.

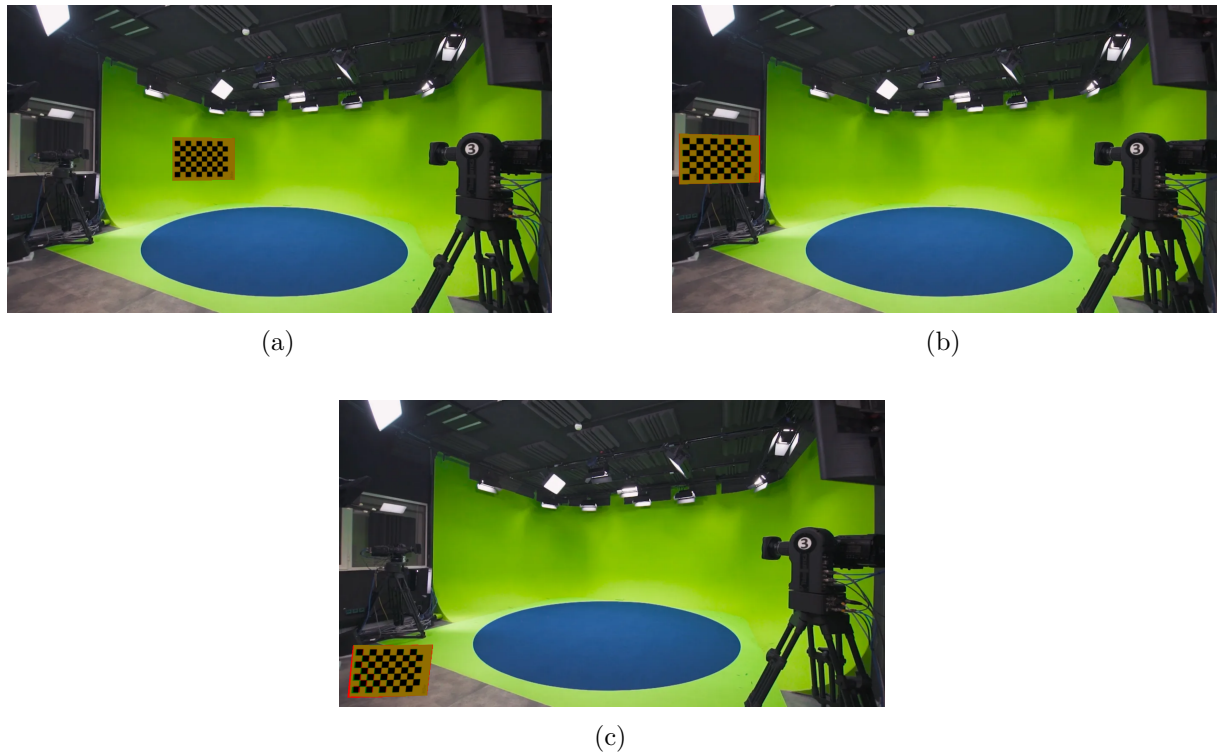


Figure 9.6: Zoom 3 Focus 2 - (a) FoV, (b) K1, (c) K2.

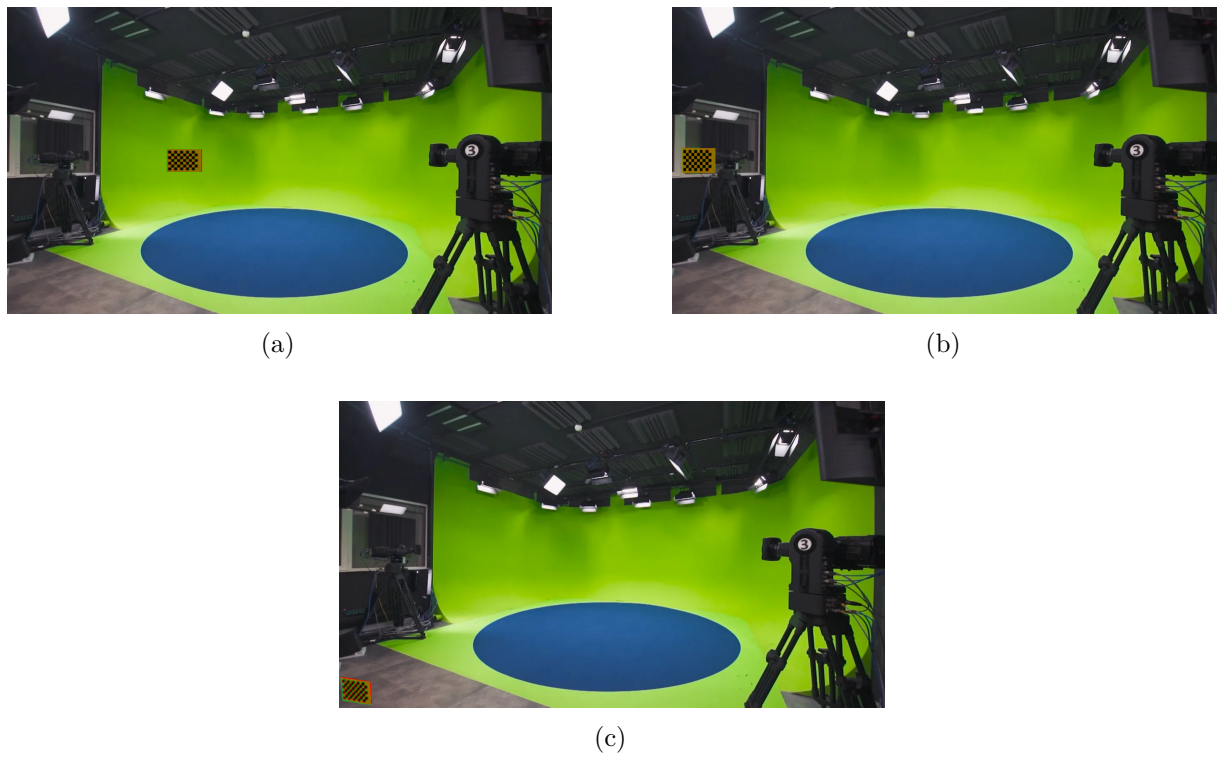


Figure 9.7: Zoom 4 Focus 1 - (a) FoV, (b) K1, (c) K2.

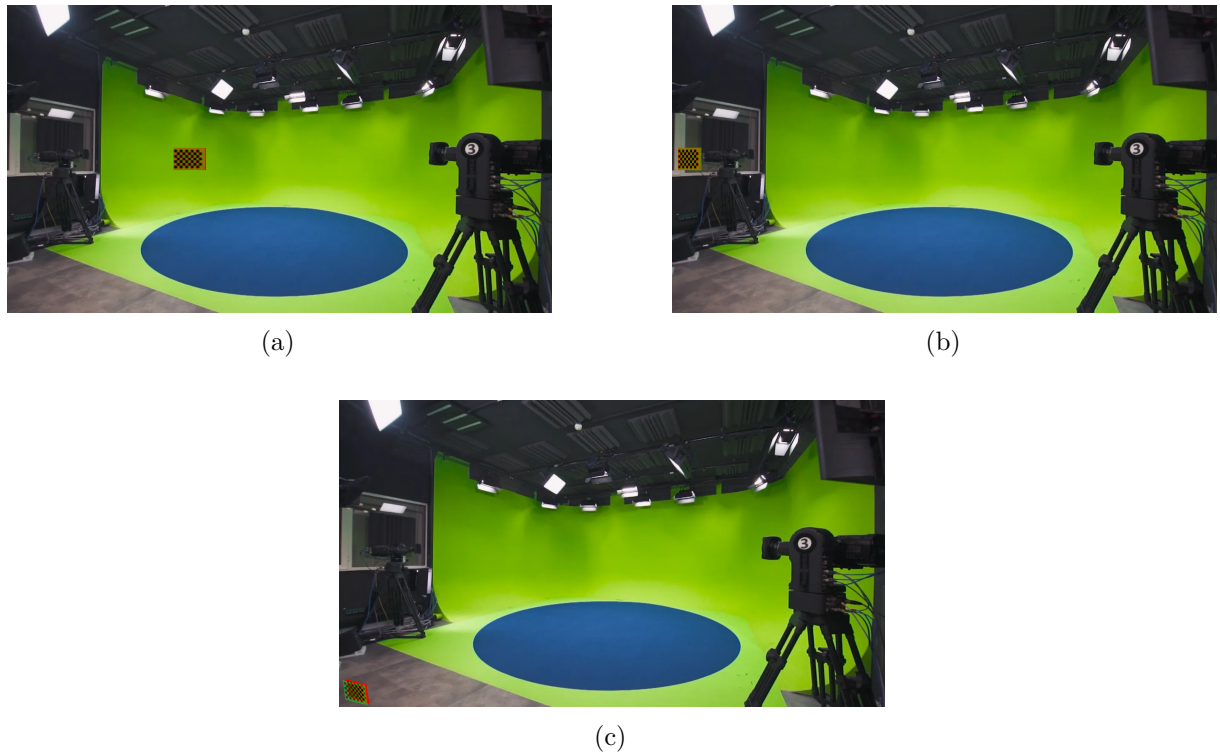


Figure 9.8: Zoom 4 Focus 2 - (a) FoV, (b) K1, (c) K2.

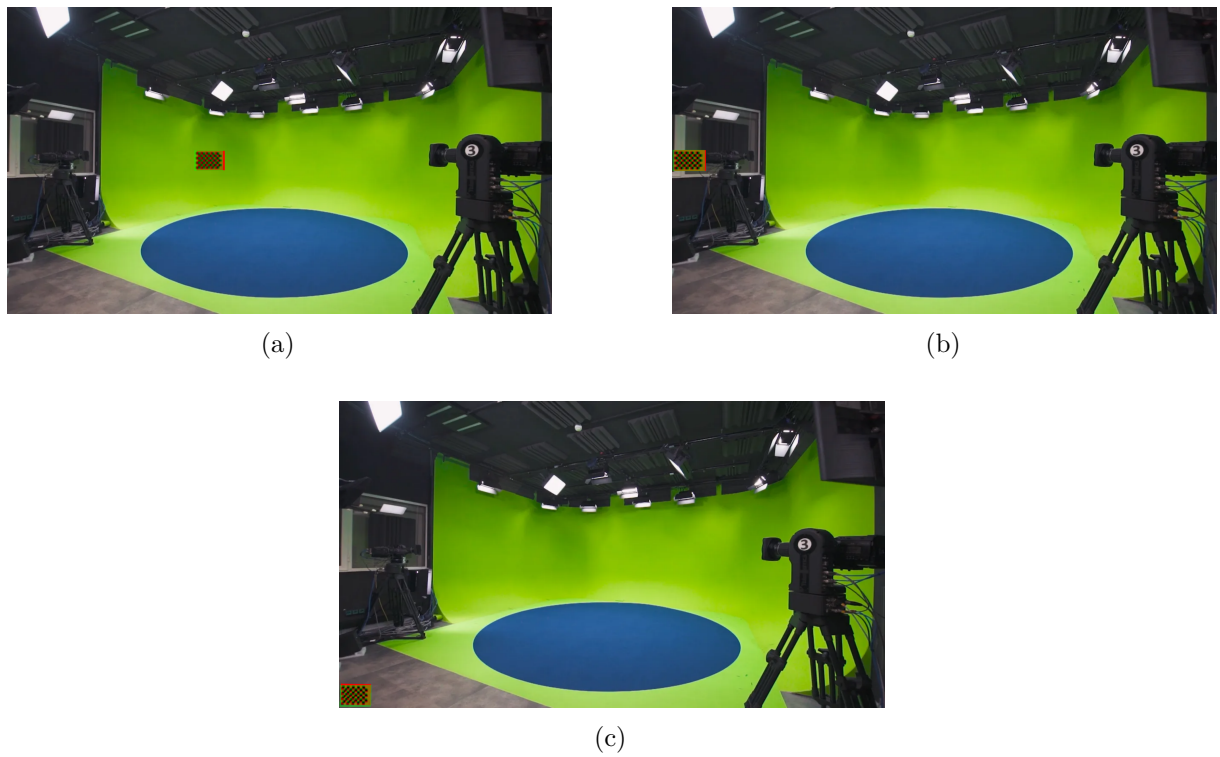


Figure 9.9: Zoom 5 Focus 1 - (a) FoV, (b) K1, (c) K2.

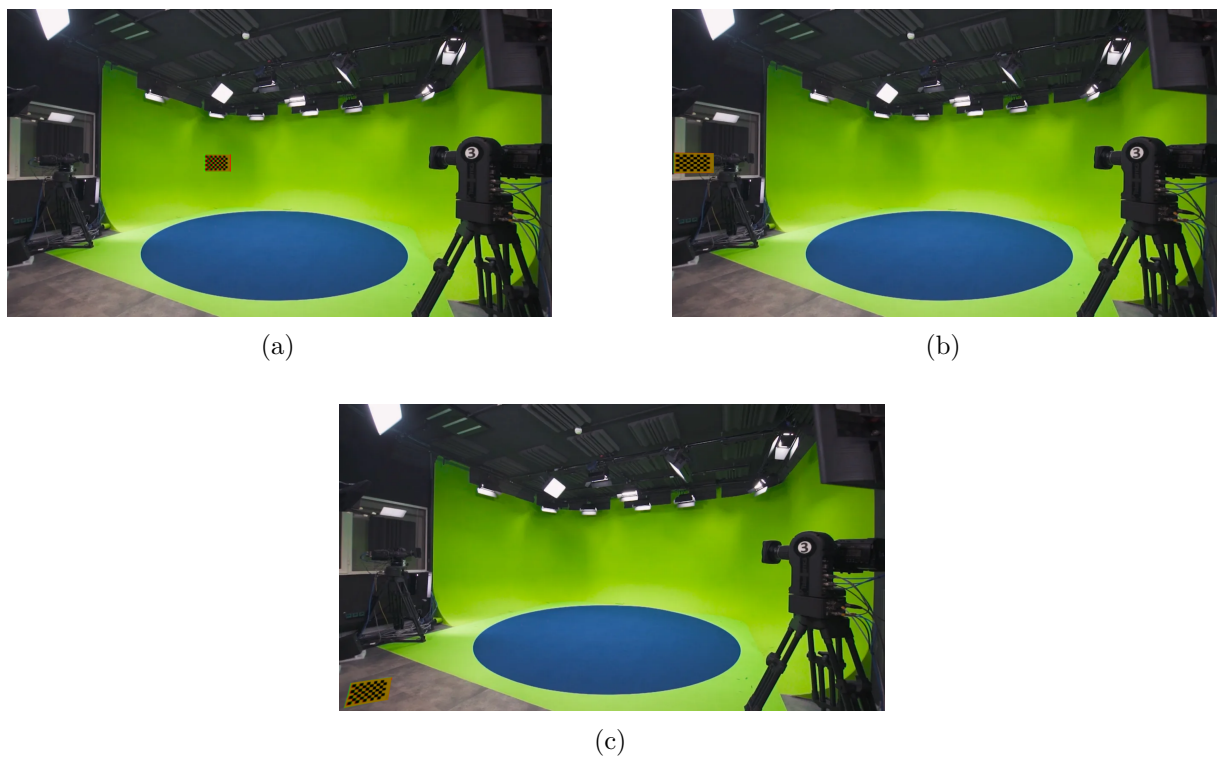


Figure 9.10: Zoom 5 Focus 2 - (a) FoV, (b) K1, (c) K2.

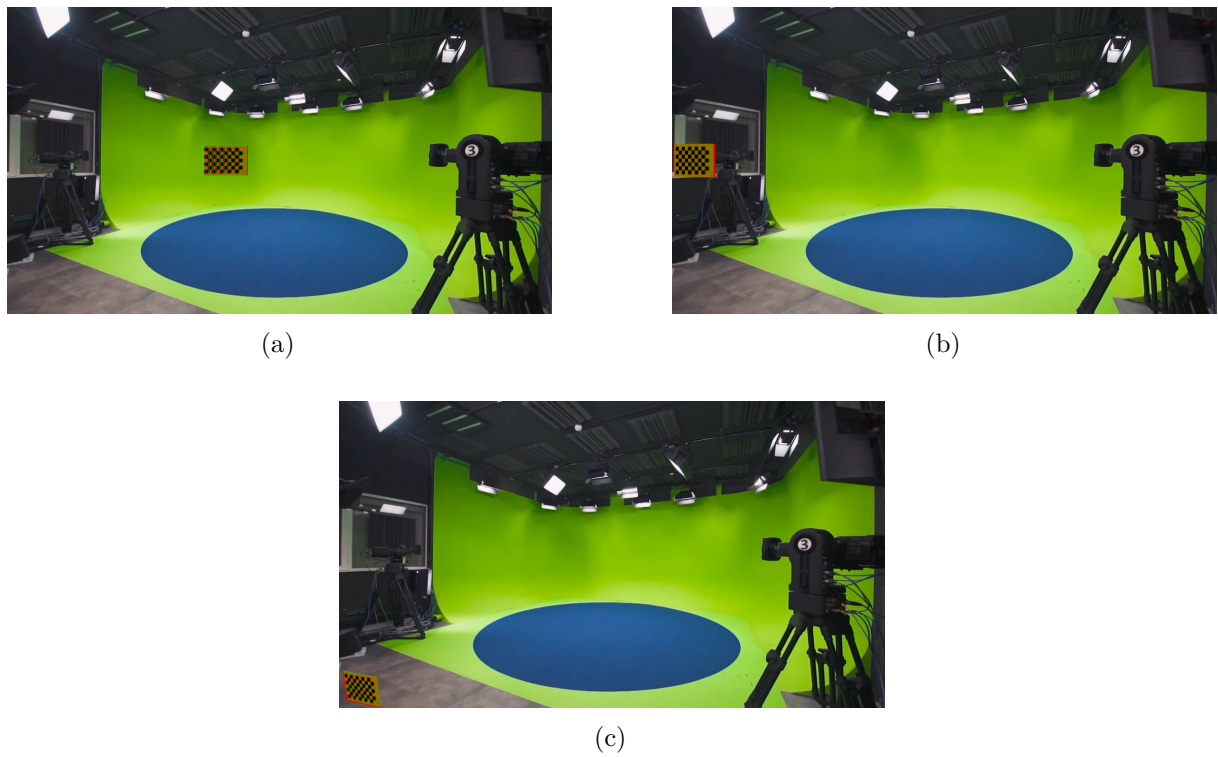


Figure 9.11: Zoom 6 Focus 1 - (a) FoV, (b) K1, (c) K2.

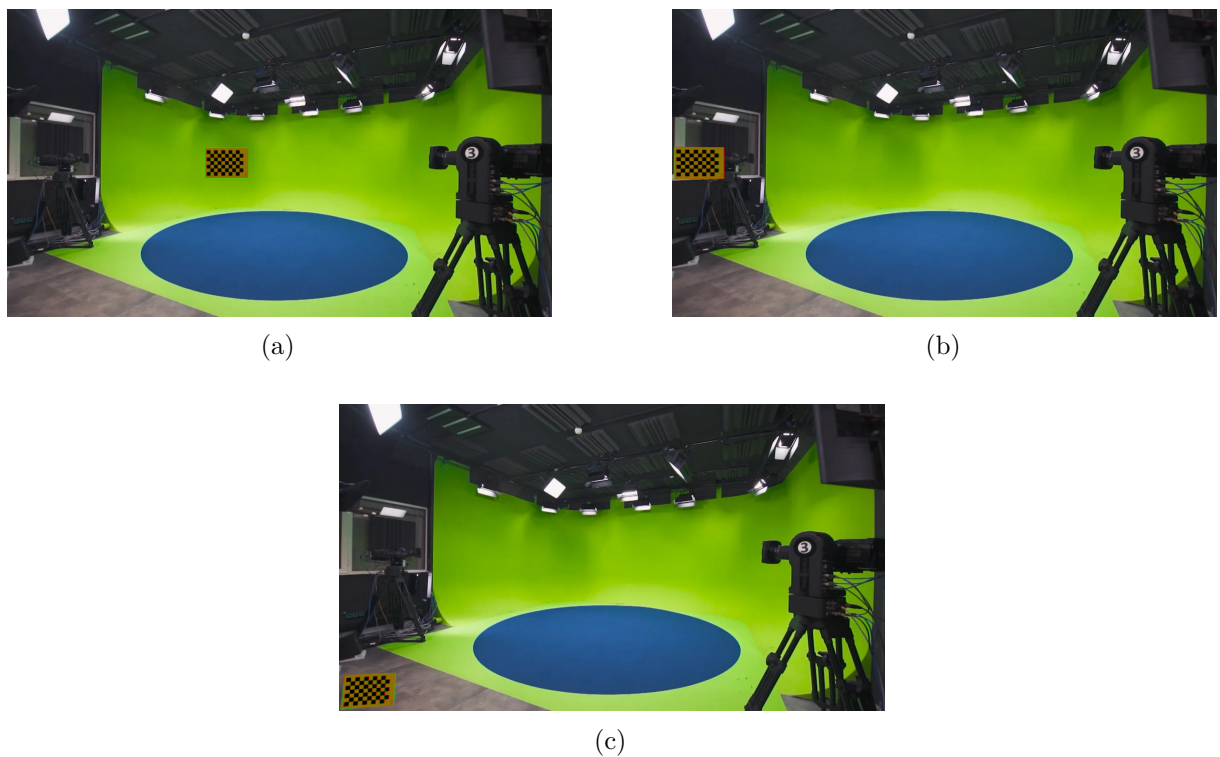


Figure 9.12: Zoom 6 Focus 2 - (a) FoV, (b) K1, (c) K2.

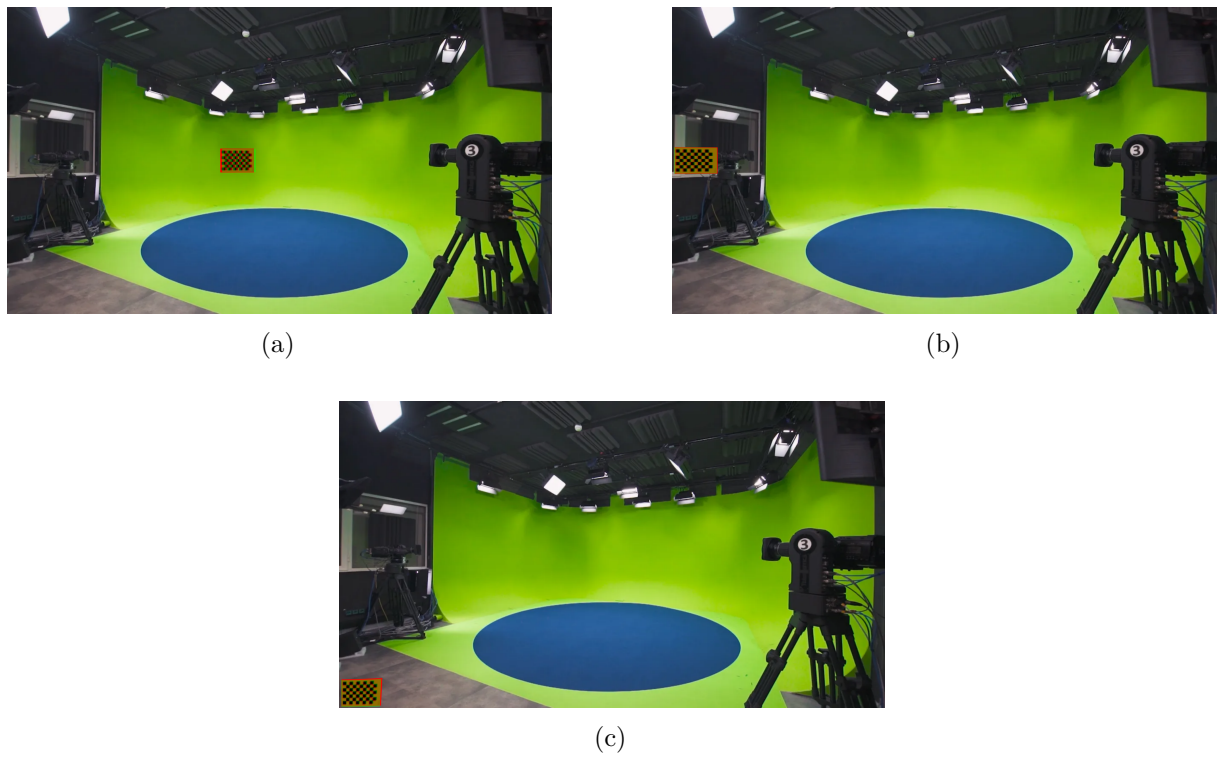


Figure 9.13: Zoom 7 Focus 1 - (a) FoV, (b) K1, (c) K2.

Bibliography

- [1] GeeksforGeeks. [Opencv contour approximation](#), 2023.
- [2] W. Richard Stevens, Bill Fenner, and Andrew M. Rudoff. *UNIX Network Programming, Volume 1: The Sockets Networking API*. Addison-Wesley Professional, 2003.
- [3] Abraham Silberschatz, Peter B. Galvin, and Greg Gagne. *Operating System Concepts*. Wiley, 2018.
- [4] Beej Jorgensen. [Beej's guide to network programming](#), 2023.
- [5] Python Software Foundation. [socket — low-level networking interface](#), 2023.
- [6] D.C. Brown. Decentering distortion of lenses. *Photogrammetric Engineering*, 32(3):444–462, 1966.
- [7] Scott Workman, Connor Greenwell, Menghua Zhai, Richard Baltenberger, and Nathan Jacobs. Deepfocal: A method for direct estimation of focal length from images. In *British Machine Vision Conference (BMVC)*, 2015.
- [8] Yannick Hold-Geoffroy, Kalyan Sunkavalli, Saurabh Hadap, Eli Shechtman, and Jean-François Lalonde. A perceptual measure for deep single image camera calibration. In *CVPR*, 2018.
- [9] Manuel Lopez-Antequera, Rafael Muñoz-Salinas, Ricardo Medina-Carnicer, and Enrique Yeguas-Bolivar. Geometry-aware learning of camera parameters from single images. In *CVPR*, 2019.
- [10] Kaiming He, Xiangyu Zhang, Shaoqing Ren, and Jian Sun. Deep residual learning for image recognition. In *CVPR*, 2016.

- [11] Jian Sun, Wenqi Cao, Zongben Xu, and Jean Ponce. Learning a convolutional neural network for non-uniform motion blur removal. *CVPR*, 2015.
- [12] Seungjun Nah, Tae Hyun Kim, and Kyoung Mu Lee. Deep multi-scale convolutional neural network for dynamic scene deblurring. In *CVPR*, 2017.
- [13] Xin Tao, Hongyun Gao, Xiaoyong Shen, Jue Wang, and Jiaya Jia. Scale-recurrent network for deep image deblurring. In *CVPR*, 2018.
- [14] Christian et al. Ledig. Photo-realistic single image super-resolution using a generative adversarial network. In *CVPR*, 2017.
- [15] Bee Lim, Sanghyun Son, Heewon Kim, Seungjun Nah, and Kyoung Mu Lee. Enhanced deep residual networks for single image super-resolution. In *CVPR Workshops*, 2017.
- [16] Orest Kupyn, Volodymyr Budzan, Mykola Mykhailych, Dmytro Mishkin, and Jiri Matas. Deblurgan: Blind motion deblurring using conditional adversarial networks. *CVPR*, 2018.
- [17] Justin Johnson, Alexandre Alahi, and Li Fei-Fei. Perceptual losses for real-time style transfer and super-resolution. *ECCV*, 2016.
- [18] Orest et al. Kupyn. Deblurgan-v2: Deblurring (orders-of-magnitude) faster and better. *ICCV*, 2019.
- [19] Hang Zhao, Orazio Gallo, Iuri Frosio, and Jan Kautz. Loss functions for image restoration with neural networks. *IEEE Trans. on Computational Imaging*, 2017.
- [20] Zhou Wang, Alan C. Bovik, Hamid R. Sheikh, and Eero P. Simoncelli. Image quality assessment: from error visibility to structural similarity. *IEEE Trans. Image Process.*, 2004.
- [21] Zhendong et al. Wang. Uformer: A unified transformer for efficient low-level vision. In *CVPR*, 2022.
- [22] Syed Waqas et al. Zamir. Restormer: Efficient transformer for high-resolution image restoration. In *CVPR*, 2022.
- [23] OpenCV Documentation. [Canny edge detection](#), 2023.
- [24] pyimagesearch. [Python | opencv canny function](#), 2021.
- [25] OpenCV. [Contour features](#).

- [26] Xuetong Yin, Jianping Wang, and Tao Xiang. Fisheyedistortionnet: Self-supervised calibration via photometric error minimization. In *ECCV*, 2018.
- [27] Bolei Zhou, Agata Lapedriza, Aditya Khosla, Aude Oliva, and Antonio Torralba. Places: A 10 million image database for scene recognition. *IEEE Transactions on Pattern Analysis and Machine Intelligence*, 40(6):1452–1464, 2017.
- [28] Zhengyou Zhang. A flexible new technique for camera calibration. *IEEE Transactions on Pattern Analysis and Machine Intelligence*, 22(11):1330–1334, 2000.
- [29] Areeb Chaudhry, Anas Rahman, and Feng Zhou. Single-image brown-conrady camera calibration with resnet regression. In *CVPR*, 2024.
- [30] A. E. Conrady. Decentering lens systems. *Monthly Notices of the Royal Astronomical Society*, 79(5):384–390, 1919.
- [31] Yuanzhou Rong, Yilin Wang, Yi Yang, and Dacheng Tao. Radial distortion correction using convolutional neural networks trained with synthetic data. In *International Conference on Multimedia and Expo (ICME)*, 2016.